THÈSE DE DOCTORAT

École Polytechnique

# Preconditioning Integral Equations on Singular Domains

MARTIN AVERSENG

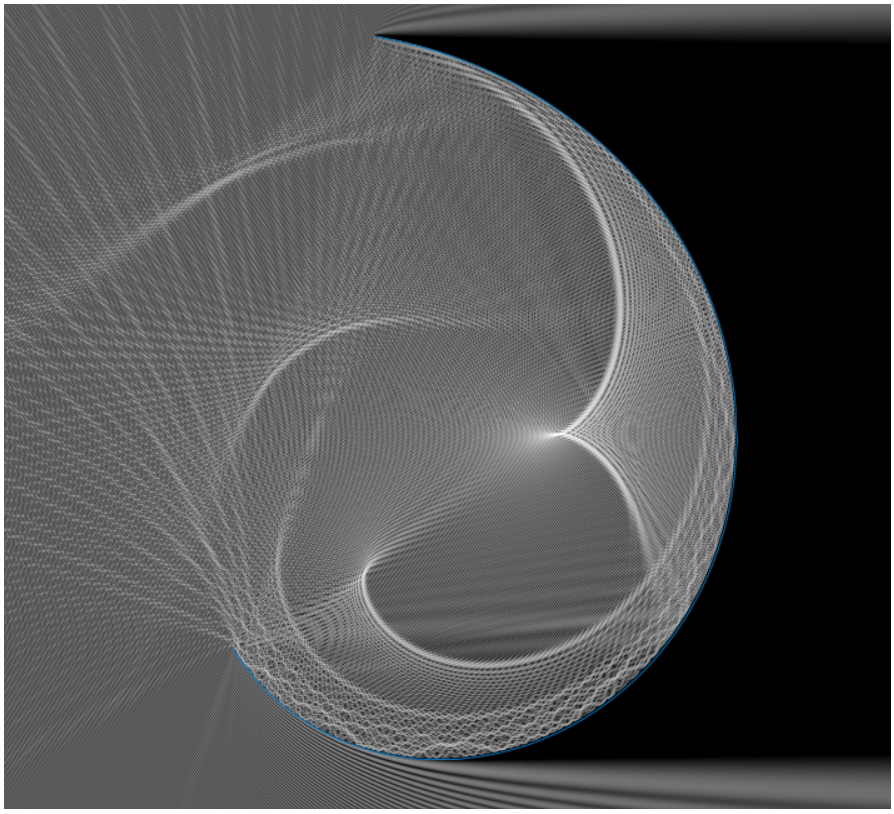

Thèse effectuée au CMAP, École Polytechnique
Sous la direction de Pr. François Alouges.

# Contents

# Introduction (français)

# Introduction (english)

# Chapter 1

# Efficient Bessel Decomposition

**Abstract:** We introduce a new algorithm for the fast evaluation of discrete convolutions with radial kernels in $\mathbb{R}^2$ using the Non-Uniform Fast Fourier Transform. In contrast with other approaches, a Fourier representation of the kernel is obtained with frequency samples lying on concentric circles rather than on a Cartesian grid. As a consequence, we require much less terms to reach a given accuracy. This allows for a faster evaluation of the discrete convolution at the cost of longer precomputations. We provide a full analysis of the complexity and error of our method. Numerical results are reported.

## Introduction

We describe a fast algorithm for computing discrete convolutions of the form

$$q_k = \sum_{l=1}^{N_z} G(z_k - z_l) f_l \,, \quad k \in \{1, \cdots, N_z\} \,. \tag{1.1}$$

when $G$ is a radial function, i.e. there exists a function $g : \mathbb{R}^+ \to \mathbb{R}$ such that, for almost all $x \in \mathbb{R}^3$, $G(x) = g(|x|)$, where $|\cdot|$ denotes the Euclidean norm. To simplify the notation, we write in such a case $G(x) = G(r)$ where $r = |x|$. We assume that the nodes $z = (z_k)_{1 \le k \le N_z}$ lie inside a disk of radius $\delta_{\max}$ in $\mathbb{R}^2$. Finally $f = (f_k)_{1 \le k \le N_z}$ is a complex vector. For example, in the resolution of the Laplace equation with Dirichlet boundary conditions by the boundary integral method with a Krylov one needs to compute many discrete convolutions like Equation (1.1) with $G(x) = -\frac{1}{2\pi} \log |x|$, the kernel of the single layer potential (when the kernel is singular, we take the convention $G(0) = 0$ in the convolution (1.1)). Their computation are a bottleneck in this method. Discrete convolutions also appear in multiple other fields of mathematics and physics, such as particle simulation, biochemistry, tomography etc.

In principle, the effective computation of the vector $q = (q_k)_{1 \le k \le N_z}$ using Equation (1.1) requires $N_z^2$ evaluations of the kernel. However, several more efficient algorithms have emerged to compute an approximation of $q$ with only quasilinear complexity in $N_z$. Among those is the celebrated Fast Multipole Method (FMM, see for example [8, 9, 14, 22, 23] and references therein). Although this algorithm is very efficient, it suffers from complicated and kernel-specific implementation. For a radial kernel and a 2-dimensional problem, Potts and Steidl [20] introduced an algorithm, which we

call here *Fastsum*, that is both simpler and more versatile than the FMM, while achieving comparable performances.

This method relies on the Non-Uniform Fast Fourier Transform (NUFFT, see the seminal paper [12] and also [15, 16, 19, 21] and references therein for tutorials, numerical aspects and open source codes) to convert the convolution (1.1) into a product in frequency space. The NUFFT takes as inputs a set of $N_z$ nodes $z$ and $N_\xi$ frequency samples $\xi$ in $\mathbb{R}^2$, a complex vector $\alpha \in \mathbb{C}^{N_z}$ and returns the vector $u \in \mathbb{C}^{N_\xi}$ defined by:

$$u_\nu = \sum_{k=1}^{N_z} e^{\pm i z_k \cdot \xi_\nu} \alpha_k \,, \quad \nu \in \{1, \cdots, N_\xi\} \,.$$

We denote the resulting vector $u$ by $\mathrm{NUFFT}_\pm[z,\xi](\alpha)$. This algorithm generalizes the classical Fast Fourier Transform (FFT, [10]) to nonequispaced data, preserving the quasi-linear complexity.

*Fastsum* exploits the NUFFT as follows. A trigonometric representation of the kernel $G$ is derived:

$$G(x) \approx G_{\mathrm{trig}}(x) := \sum_{\nu=1}^{N_\xi} e^{ix\cdot\xi_\nu} \hat{\omega}_\nu \,, \tag{1.2}$$

where $(\xi_\nu)_{\nu=1\cdots N_\xi}$ are the frequency samples in $\mathbb{R}^2$ and $\hat{\omega}_\nu$ are complex numbers. This representation is replaced in (1.1) to yield the fast approximation

$$\begin{aligned} q_k &\approx \left( \sum_{\nu=1}^{N_\xi} e^{+iz_k\cdot\xi_\nu} \left[ \hat{\omega}_\nu \sum_{l=1}^{N_z} e^{-iz_l\cdot\xi_\nu} f_l) \right] \right)_{1\le k\le N_z} \\ &= \mathrm{NUFFT}_+[z,\xi]\left(\hat{\omega} \odot \mathrm{NUFFT}_-[z,\xi](f)\right), \end{aligned} \tag{1.3}$$

where $\odot$ denotes the element wise product between vectors.

For 3 space dimensions, an analog method was developed by Alouges and Aussal, named the Sparse Cardinal Sine Decomposition (SCSD). The main difference lies in the choice of the frequency samples in the representation (1.2). Instead of choosing them on a Cartesian grid like *Fastsum*, the SCSD allows for nonequispaced frequencies and seeks a trigonometric representation with the smallest possible number of terms. This non-linear and high-dimensional minimization problem is made tractable by exploiting the radial symmetry of the problem.

The aim of this work is to adapt the SCSD method to 2 space dimensions. The cardinal sines must be replaced by Bessel functions and the frequencies are chosen on a set of concentric circles centered at the origin. We obtain trigonometric representations with much fewer terms than in *Fastsum*. Since the frequencies are no longer equispaced, the slower NUFFT of type 3 must be used instead of type 1 (following the terminology of [17]). Nevertheless, the numerical tests, exposed in Section 1.7, show that the gain in number of frequency samples leads to a faster evaluation of (1.1), at the cost of longer precomputations.

The remainder of the paper is organized as follows. We first give a self-contained description of our algorithm in Section 1.1, and state its complexity in Theorem 1.1 in a special case. Then, Section 1.2 briefly presents the theory of Fourier-Bessel decomposition. In Section 1.3, we analyze the "Efficient Bessel Decomposition" (EBD), a new method to approximate singular kernels by Bessel series outside the origin with only a small number of terms. In Section 1.4, we estimate the number of terms required in the EBD to reach a given accuracy for the logarithmic kernel. We also describe how to deal with other kernels. In Section 1.5, we show how to convert a Bessel decomposition into a trigonometric polynomial through what we call "circular quadratures". In Section 1.6, we summarize

the complexity of each step and prove Theorem 1.1. We finally give a numerical comparison of our algorithm with *Fastsum*.

A Matlab code of the method described here is available online [5].

## 1.1 Summary of the algorithm

### 1.1.1 Trigonometric representation

In this section, given a cut-off parameter $\delta_{\min} > 0$ (also recall $\delta_{\max}$ is the diameter of the set of nodes $z$), we describe how to select the frequency samples $(\xi_v)$ in the trigonometric representation (1.2).

**Efficient Bessel Decomposition.** We first reduce to a 1-dimensional approximation problem. We find a linear combination of Bessel functions approximating $G(r)$ on $[\delta_{\min}, \delta_{\max}]$:

$$G(r) \approx G(\delta_{\max}) + \sum_{p=1}^{P} \alpha_p J_0\left(\rho_p \frac{r}{\delta_{\max}}\right), \quad r \in [\delta_{\min}, \delta_{\max}], \tag{1.1.1}$$

where $J_0$ is the Bessel function of first kind and zero order and $(\rho_p)$ is the sequence of its roots (see Definition 1.1 for more details). We choose $\alpha_1, \cdots, \alpha_P$ as the minimizers of the least square error

$$E(\alpha_1, \cdots, \alpha_P) = \int_{\delta_{\min}}^{\delta_{\max}} r \left[\frac{d}{dr}\left(G(r) - \sum_{p=1}^{P} \alpha_p J_0\left(\rho_p \frac{r}{\delta_{\max}}\right)\right)\right]^2 dr.$$

The number of terms $P$ is chosen as the smallest integer for which the $L^\infty$ error is below a given tolerance. This amounts to solving a series of linear systems where the matrix coefficients are explicit (see Theorem 1.2). The right-hand side can be approximated by numerical quadrature when an explicit formula is not available. In Section 1.3.2, we show how to compute the vector $(\alpha_p)$ with the minimal length without solving a full linear system for each candidate $P$.

**Circular quadrature.** In a second step, we write for each $p \in \{1, \cdots, P\}$

$$J_0(\rho_p |x|) \approx \frac{1}{M_p} \sum_{m=0}^{M_p - 1} e^{i\rho_p \xi_p^m \cdot x}, \tag{1.1.2}$$

where $\xi_p^m = \left(\cos\left(\frac{2\pi m}{M_p}\right), \sin\left(\frac{2\pi m}{M_p}\right)\right)$. This is the trapezoidal rule applied to the identity

$$J_0(\rho_p |x|) = \frac{1}{2\pi} \int_{|\xi|=1} e^{i\rho_p x \cdot \xi} d\sigma(\xi).$$

The trigonometric representation (1.2) is obtained by combining Equations (1.1.1) and (1.1.2). A criterion for choosing the number of terms $M_p$ is derived in Section 1.5.

### 1.1.2 Description of the algorithm and complexity

The full algorithm is split into two parts:

**Offline part.**

**Inputs:** A radial kernel $G$, a set of $N_z$ nodes $z$ in $\mathbb{R}^2$ of diameter $\delta_{\max}$, a cut-off parameter $\delta_{\min}$ and a tolerance $\varepsilon > 0$.

**Trigonometric representation:** Combine the Bessel decomposition and the circular quadrature to obtain the trigonometric representation $G_{\text{trig}}$ of $G$, as in Equation (1.2). This approximation is valid for $\delta_{\min} \leq r \leq \delta_{\max}$ up to the tolerance $\varepsilon$.

**Correction Matrix:** Determine the set $\mathscr{P}$ of all the pairs $(k,l)$ such that $|z_k - z_l| \leq \delta_{\min}$ (fixed-radius neighbor search). Assemble the close correction sparse matrix:

$$D_{kl} = \delta_{(k,l)\in\mathscr{P}} \left( G(z_k - z_l) - G(\delta_{\max}) - \sum_{p=1}^{P} \alpha_p J_0 \left( \rho_p \frac{|z_k - z_l|}{\delta_{\max}} \right) \right). \tag{1.1.3}$$

The last two terms inside the parentheses counteract the error introduced by the approximation of $G$ in Bessel series near the origin. The last sum is computed efficiently using a piecewise polynomial interpolation of the function

$$r \mapsto \sum_{p=1}^{P} \alpha_p J_0(\rho_p r), \quad r \in (0, \delta_{\min}).$$

**Outputs**: The set of weights $(\hat{\omega}_\nu)$, the frequency samples $(\xi_\nu)$ and the (sparse) correction matrix $D$.

**Online part.**

**Inputs:** We take in input all outputs of the offline part, and a complex vector $f$ of size $N_z$.

**Far approximation:** Compute

$$q_k^{\text{far}} = \sum_{l=1}^{N_z} G_{\text{trig}}(z_k - z_l) f_l, \quad 1 \leq k \leq N_z \tag{1.1.4}$$

in the following three steps:

(i) **Space $\to$ Fourier:** Compute $\hat{f} = \text{NUFFT}_-[z,\xi](f)$.

(ii) **Fourier multiply:** Perform an element-wise multiplication by $\hat{\omega}$:

$$\hat{g}_\nu := \hat{\omega}_\nu \hat{f}_\nu.$$

(iii) **Fourier $\to$ Space:** Compute $q^{\text{far}} = \text{NUFFT}_+[z,\xi](\hat{g})$.

**Close correction:** Compute the sparse matrix product:

$$q^{\text{close}} = Df.$$

**Output:** The vector $q = q^{\text{far}} + q^{\text{close}}$, with, for any $k \in \{1, \cdots, N_z\}$,

$$\left| q_k - \sum_{l=1}^{N_z} G(z_k - z_l) f_l \right| \leq \varepsilon \sum_{l=1}^{N_z} |f_l|.$$

For the special case of the logarithmic kernel and for nodes uniformly distributed on a curve, the complexity of the algorithm is given by the following theorem, which is proved in Section 1.6.

**Theorem 1.1.** *Assume the nodes $(z_k)$ are uniformly distributed on a regular curve, and $G(x) = \log|x|$. Let $\varepsilon > 0$ the desired accuracy of the method. Let*

$$a = \frac{1}{N_z^{2/3-\eta}}$$

*for some $\eta \in \left[0, \frac{1}{6}\right]$, and choose*

$$\delta_{\min} = a\delta_{\max}\,.$$

*Then there exists a constant $C > 0$ independent of $N_z$, $\varepsilon$ and $\eta$ such that:*

*(i) The number of operations required for the computation of the trigonometric representation* (1.2) *valid for $|x| \in [\delta_{\min}, \delta_{\max}]$ is bounded by*

$$C_{\text{off}}(N_z, \varepsilon, \eta) \leq C\,|\log\varepsilon|^3\, N_z^{2-3\eta}\,,$$

*(ii) The number of operations required for the assembling of the close correction matrix $D$ is bounded by*

$$C_{\text{assemble}}(N_z, \varepsilon, \eta) \leq C N_z^{4/3+\eta}\,,$$

*(iii) Once these two steps have been completed, the discrete convolution* (1.1) *can be evaluated for any choice of vector $f$ at a precision at least $\varepsilon \sum_l |f_l|$ in a number of operations bounded by*

$$C_{\text{on}}(N_z, \varepsilon, \eta) \leq C\left(N_z^{4/3+\eta} + N_z^{4/3-2\eta}\log(N_z)\,|\log\varepsilon|^4\right).$$

The choice for the parameter $a$ depends on the distribution of nodes $z$. For example, for data uniformly distributed on a disk, if we choose $a \propto \frac{1}{\sqrt{N_z}}$ we obtain complexities of $O(|\log\varepsilon|^3 N_z^{3/2})$ and $O(|\log\varepsilon|^4 N_z \log(N_z))$ for the offline and online parts respectively.

## 1.2 Series of Bessel functions and error estimates

In this section, we give a short introduction to Fourier-Bessel series as an orthonormal decomposition on the eigenfunctions of the Laplace operator, and study the truncation error for smooth functions. We suggest [3, 27] and [26, chap. 18] for background. The main result needed for our purpose is Theorem 1.3.

Our method can be adapted for any space dimension. For example, in $\mathbb{R}^3$ the radial eigenvalues of the Laplace operator are proportional to

$$x \mapsto \frac{J_{1/2}(2\pi p\,|x|)}{|x|^{1/2}}, \quad p \in \mathbb{N}^*.$$

In other words, our approach generalizes [4] to any dimension.

### 1.2.1 Radial eigenfunctions of Laplace's operator with Dirichlet boundary conditions

In the following, $B$ denotes the unit ball in $\mathbb{R}^2$ and $\partial B$ its boundary. Let $L^2_{\text{rad}}(B)$ the space of those functions in $L^2(B)$ that are radial and

$$C^\infty_{c,\text{rad}}(B) = \{\varphi \in C^\infty_c(B) \mid \varphi \text{ is radial } \}\,.$$

Similarly, let $H^1_{\text{rad}}(B) = H^1(B) \cap L^2_{\text{rad}}(B)$, where $H^1(B)$ is the usual Sobolev space of square integrable functions with square integrable weak derivatives. $H^1_{\text{rad}}(B)$ is a Hilbert space for the norm

$$\|u\|^2_{H^1_{\text{rad}}(B)} = \int_B |u(x)|^2 + |\nabla u(x)|^2\,dx = 2\pi \int_0^1 r\left(u(r)^2 + u'(r)^2\right)dr\,.$$

Finally, $H^1_{0,\text{rad}}(B)$ is the closure of $C^\infty_{c,\text{rad}}(B)$ in $H^1_{\text{rad}}(B)$, with the equivalent norm

$$\|u\|^2_{H^1_{0,\text{rad}}(B)} = 2\pi \int_0^1 r u'(r)^2 dr\,.$$

We now briefly recall some facts on Bessel functions.

**Definition 1.1.** The Bessel function of the first kind and order $\alpha$, $J_\alpha$ is defined by the power series:

$$J_\alpha(r) := \sum_{m=0}^{\infty} \frac{(-1)^m}{m!\,\Gamma(m+1+\alpha)} \left(\frac{r}{2}\right)^{2m+\alpha}. \tag{1.2.1}$$

The roots $(\rho_p)_{p\in\mathbb{N}^*}$ of $J_0$, behave for large $p$ as

$$\rho_p \underset{p\to\infty}{\sim} \pi p\,.$$

For any $p \in \mathbb{N}^*$, we introduce:

$$e_p(x) = C_p J_0(\rho_p\,|x|)\,,$$

where the normalization constant $C_p$ is chosen such that $\|e_p\|_{H^1_0(B)} = 1$, that is

$$C_p = \frac{1}{\left(2\pi \int_B r\rho_p^2 J_1(\rho_p r)^2\right)^{1/2}} = \frac{1}{\sqrt{\pi}\rho_p\,|J_1(\rho_p)|}\,.$$

One can check, using asymptotic expansions of Bessel functions, (see for example equations (10.17.1 - 10.17.3) in [27]) that

$$C_p = \frac{1}{\sqrt{2\pi p}} + O\left(\frac{1}{p^{3/2}}\right), \tag{1.2.2}$$

For any $p \in \mathbb{N}^*$, $e_p$ satisfies:

$$-\Delta e_p = \rho_p^2 e_p\,. \tag{1.2.3}$$

In the sequel, we denote by $\mathscr{A}(a)$ the annulus

$$\mathscr{A}(a) = \left\{x \in \mathbb{R}^2 \;\middle|\; |x| \le a\right\}.$$

**Theorem 1.2.** *The family $\{e_p \mid p \in \mathbb{N}^*\}$ is a Hilbert basis of $H^1_{0,\mathrm{rad}}(B)$. For $0 \le a \le 1$, the $H^1_0$ scalar product on the annulus $\mathscr{A}(a)$ of two eigenfunctions is given by the following formulae:*

$$\int_{\mathscr{A}(a)} \nabla e_i \cdot \nabla e_j = \frac{2\pi C_i C_j \rho_i \rho_j}{\rho_j^2 - \rho_i^2} \Big[ F_{i,j}(1) - F_{j,i}(1) - F_{i,j}(a) + F_{j,i}(a) \Big]$$

*if $i \neq j$, where*

$$F_{i,j}(r) = \rho_i r J_0(\rho_i r) J_0'(\rho_j r)\,,$$

*while*

$$\int_{\mathscr{A}(a)} |\nabla e_i|^2 = 2\pi C_i^2 \big( F_i(1) - F_i(a) \big)$$

*where*

$$F_i(r) = \rho_i^2 r^2 \left[ \frac{1}{2} J_0(\rho_i r)^2 + \frac{1}{2} J_0'(\rho_i r)^2 \right] + \rho_i r J_0(\rho_i r) J_0'(\rho_i r)\,.$$

*Proof.* The Laplace operator is self-adjoint, positive definite on $H^1_0(B)$ thus its normalized eigenfunctions form a Hilbert basis of this space. Their expression is given in [13, Eq. (3.9)] in polar coordinates $(r, \varphi)$ by

$$u_{nkl}(r,\varphi) = J_n(j_{nk} r) \begin{cases} \cos(n\varphi) & l = 1, \\ \sin(n\varphi) & l = 2 \ (n \neq 0)\,. \end{cases}$$

where $j_{nk}$ is the $k$-th positive root of $J_n$. The fact that $(e_p)$ is a Hilbert basis of $H^1_{0,\mathrm{rad}}(B)$ stems from the observation that the radial functions are $H^1_0$ orthogonal to $u_{nkl}$ as soon as $n \neq 0$. The scalar product formulae can be verified by differentiating the functions $F_{i,j}$ and $F_i$.

□

### 1.2.2 Truncation error for smooth functions

We now present the Fourier-Bessel series and prove a bound for the truncation error. First of all, Theorem 1.2 implies that any function $f \in H^1_{0,\mathrm{rad}}(B)$ can be expanded through its so-called Fourier-Bessel series as

$$f = \sum_{p \in \mathbb{N}^*} c_p(f) e_p\,,$$

where the "Fourier-Bessel" coefficients $c_p(f)$ are given by

$$c_p(f) = \int_B \nabla f(x) \cdot \nabla e_p(x) dx = \rho_p^2 C_p \int_0^1 r f(r) J_0(\rho_p r) dr\,.$$

See for example [26, Chap. 18, Eq. (2)]. Notice the second equality is obtained by integration by part. We will show that the coefficients decay rapidly when $f$ is smooth. To this aim, we first introduce the following terminology:

**Definition 1.2.** A radial function $f$ satisfies the multi-Dirichlet condition of order $n \in \mathbb{N}^*$ if $f$ is $H^{2n}$ in a neighborhood of $\partial B$ and if for all $s \le n-1$, the $s$-th iterate of $-\Delta$ on $f$, $(-\Delta)^s f$, vanishes on $\partial B$ (with the convention $(-\Delta)^0 f = f$).

An equivalent statement of the following result can be found in [24, Chap. 8, Sec. 20, Thm. 1]. The proof is reproduced here for the reader's convenience.

**Proposition 1.3.** *If $f \in H^{2n}(B)$ satisfies the multi-Dirichlet condition of order n, then for any $p \in \mathbb{N}^*$:*

$$c_p(f) = \frac{1}{\rho_p^{2n-2}} \int_B (-\Delta)^n f(x) e_p(x) dx.$$

*Proof.* We show this by induction. Let $f$ satisfy the multi-Dirichlet condition of order $n = 1$, then by integration by parts:

$$c_p(f) = \int_B (-\Delta) f(x) e_p(x) dx,$$

since $e_p$ vanishes on $\partial B$. Assume the result is true for some $n \geq 1$ and let $f$ satisfy the multi-Dirichlet condition of order $n+1$. Then, using $-\Delta e_p = \rho_p^2 e_p$, we get

$$c_p(f) = \frac{1}{\rho_p^{2n}} \int_B (-\Delta)^n f(x)\ (-\Delta) e_p(x) dx.$$

The result follows from integration by parts where we successively use that $(-\Delta)^n f$ and $e_p$ vanish on $\partial B$.

□

**Corollary 1.4.** *Let the remainder be defined as*

$$R_P(f) = \sum_{p=P+1}^{+\infty} c_p(f) e_p.$$

*If $f \in H^{2n}(B)$ satisfies the multi-Dirichlet condition of order n, there exists a constant C independent of n and P such that:*

$$\|R_P(f)\|_{H_0^1(B)} \leq C \frac{\|(-\Delta)^n f\|_{L^2(B)}}{(\pi P)^{2n}} \sqrt{\frac{P^3}{n}}.$$

*Proof.* Parseval's identity yields $\|R_P(f)\|^2_{H^1_{0,\mathrm{rad}}(B)} = \sum_{p=P+1}^{+\infty} |c_p(f)|^2$. By Theorem 1.3 and using $\rho_p \sim \pi p$, we can find a constant $C$ such that $|c_p(f)| \leq C \frac{\|(-\Delta)^n f\|_{L^2}}{(\pi p)^{2n-1}}$. Thus,

$$\|R_P(f)\|_{H^1_{0,\mathrm{rad}}(B)} \leq C \|(-\Delta)^n f\|_{L^2_{\mathrm{rad}}(B)} \sqrt{\sum_{p=P+1}^{+\infty} \frac{1}{(\pi p)^{4n-2}}}.$$

The announced result follows from $\displaystyle\sum_{p>P} \frac{1}{p^\alpha} \propto \frac{1}{(\alpha-1)P^{\alpha-1}}$ for $\alpha > 1$. □

### 1.2.3 Other boundary conditions

When we replace the Dirichlet boundary condition by the following Robin boundary conditions

$$\frac{\partial u}{\partial n} + Hu = 0 \tag{1.2.4}$$

for some constant $H \geq 0$, the same analysis can be conducted, leading to Dini series (also covered in [26]). This time, we construct a Hilbert basis of $H^1_{\mathrm{rad}}(B)$ with respect to the bilinear form

$$a_H(u,v) := \int_B \nabla u(x) \cdot \nabla v(x) dx + H \int_{\partial B} u(x) v(x) d\sigma(x).$$

The following result holds.

**Theorem 1.5.** *Let $(\rho_p^H)_{p\in\mathbb{N}*}$ the sequence of positive solutions of*

$$rJ_0'(r)+HJ_0(r)=0.$$

*(i) If $H>0$, the functions*

$$e_p^H(r)=C_pJ_0(\rho_p^H r),$$

*with $C_p$ such that $a_H(e_p^H,e_p^H)=1$, form a Hilbert basis of $H^1_{rad}(B)$.*

*(ii) If $H=0$, a constant function must be added to the previous family to form a complete set.*

The truncation error estimates in Theorem 1.4 can be generalized to functions satisfying multi-Robin conditions of order $n\geq 1$, that is for all $s\leq n-1$, $(-\Delta)^s u$ satisfies (1.2.4).

## 1.3 Efficient Bessel Decomposition

In this section, we describe the method for approximating a singular function outside the origin by a Fourier-Bessel series with only a few terms.

### 1.3.1 Definition

Consider the kernel $G$ involved in (1.1). We can assume up to rescaling $G$ that the diameter $\delta_{\max}$ of the nodes $z$ is 1, and therefore, we need to approximate the kernel only on the unit ball $B$. To apply the previous results, two kinds of complications may arise:

(i) When $G$ is singular near the origin, it is not in $H^{2n}(B)$ (even for $n=1$).

(ii) The multi-Dirichlet conditions may not be fulfilled up to a sufficient order.

The point (ii) is crucial in order to apply the error estimates of the previous section. The first two kernels that we will study (Laplace and Helmholtz) in the next section satisfy the favorable property:

$$\Delta G=\lambda G$$

for some $\lambda\in\mathbb{C}$, is helpful to ensure (ii) at any order. For more general kernels, we suggest a simple trick to enforce multi-Dirichlet conditions up to a given order in Section 1.4.3.

First, we deal with point (i). We avoid the singularity by approximating $G$ only in the annulus $\mathscr{A}(a)$. We look for coefficients $(\alpha_p)$ such that

$$G(r)\approx\sum_{p=1}^{P}\alpha_p e_p(r),\quad a<r<1 \tag{1.3.1}$$

for some $P>0$, where we remind the reader that $e_p$ are the radial eigenvalues of the Laplace operator on the unit ball defined in Section 1.2. We call this the Efficient Bessel Decomposition (EBD) of $G$. The EBD coefficients are chosen as the minimizers of the $H_0^1$ error on the annulus $\mathscr{A}(a)$:

$$E(\alpha_1,\alpha_2,...,\alpha_P)=\int_{\mathscr{A}(a)}\left|\nabla\left(G(x)-\sum_{p=1}^{P}\alpha_p e_p(x)\right)\right|^2 dx.$$

Given a tolerance $\varepsilon$, we choose $P$ as the smallest integer for which the $L^\infty$ error of the approximation is below $\varepsilon$. Clearly, for any radial extension $\tilde{G}$ outside the annulus $\mathscr{A}(a)$, one has

$$E(\alpha_1, \cdots, \alpha_P) \leq \left\| \tilde{G} - \sum_{p=1}^{P} c_p(\tilde{G}) e_p(x) \right\|^2_{H_0^1(B)} \tag{1.3.2}$$

In particular, when $\tilde{G}$ is smooth up to the origin, this gives an immediate error estimate via Theorem 1.4.

*Remark* 1.1. In *Fastsum*, an explicit polynomial regularization and periodisation $\tilde{G}$ is constructed and the function $G$ is replaced by the discrete Fourier expansion of $\tilde{G}$. In contrast here, the way we choose the coefficients $\alpha_p$ ensures that we get less terms than if we had constructed any particular extension $\tilde{G}$ and used $\alpha_p = c_p(\tilde{G})$.

*Remark* 1.2. In our context, the $H_0^1$ error controls the $L^\infty$ norm on $\mathscr{A}(a)$, thus ruling out any risk of Gibb's phenomenon. Indeed, for a function $u$ that vanishes on $\partial B$, one has

$$|u(x_0)| \leq \sqrt{\frac{-\log|x_0|}{2\pi}} \sqrt{\int_{\mathscr{A}(a)} |\nabla u(x)|^2 dx}, \quad \text{almost for all } x_0 \in \mathscr{A}(a),$$

as can be shown by applying the Cauchy-Schwarz inequality to $u(r) = -\int_r^1 u'(t)dt$.

### 1.3.2 Numerical computation of the EBD

**Efficient computation of the coefficients.** For a given kernel $G$ and integer $P > 0$, the EBD coefficients $\alpha_1, \cdots, \alpha_P$ are found by solving the following linear system:

$$\begin{aligned} &\sum_{q=1}^{P} \rho_q C_q \left( \int_{\mathscr{A}(a)} J_1(\rho_p|x|) J_1(\rho_q|x|) dx \right) \alpha_q \\ &= -\int_{\mathscr{A}(a)} G'(x) J_1(\rho_p|x|) dx, \quad 1 \leq p \leq P, \end{aligned} \tag{1.3.3}$$

where $J_1$ is the Bessel function of first kind and order 1 (in fact, $J_0' = -J_1$). The explicit matrix entries are given in Theorem 1.2.

Using Cholesky decomposition, it is possible to compute efficiently the solution of the system for $P'$ coefficients from the solution for a greater $P$. Indeed, for $P \in \mathbb{N}^*$, let us call $A_P$ the system matrix and $b_P$ the second member. If $C_P$ is the first Cholesky factor, then $C_{P'}$ is obtained by extracting the top left $P' \times P'$ sub-matrix of $C_P$. Moreover, $b_{P'}$ is just the vector formed of the first $P'$ entries of $b_P$. This way, once the tolerance is reached, we can efficiently remove as many terms as possible.

**Numerical stability.** Numerical evidence strongly suggests that the conditioning number ($\text{cond}_2$) of the linear system (1.3.3) only depends on the parameter $\gamma := Pa$. This is shown in Figure 1.1 where we plot the isovalues of the condition number of the system in function of $P$ and $\gamma$. One can observe the condition number is almost insensitive to the value of $P$ for constant $\gamma$.

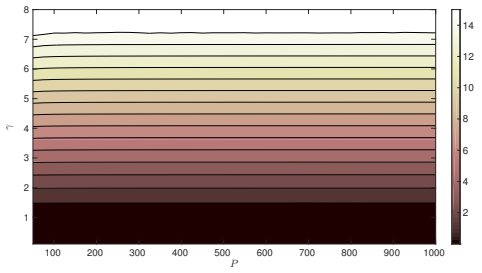


Figure 1.1: Isovalues of the function $(P,\gamma) \mapsto \log_{10}(\mathrm{cond}_2(A))$ where $A$ is the matrix of the linear system (1.3.3) and where $\gamma = Pa$.

## 1.4 Error estimates

### 1.4.1 Laplace kernel

When solving PDE's involving the Laplace operator (for example in heat conduction or electrostatic problems), one is led to (1.1) with the logarithmic kernel $G(r) = \log(r)$. Here we show that its EBD converges exponentially fast:

**Theorem 1.6.** *There exist two positive constants $L_1$ and $l_2$ such that*

$$\forall a \in (0,1), \forall P \in \mathbb{N}^*, \forall r \in (a,1), \quad \left| G(r) - \sum_{p=1}^{P} \alpha_p e_p(r) \right| \leq L_1 e^{-l_2 a P}$$

*where $\alpha_1, \cdots, \alpha_P$ are the EBD coefficients of $G$ of order $P$.*

We prove this by exhibiting an extension $\tilde{G}$ of $G$ outside the annulus $\mathscr{A}(a)$. We estimate the truncation error of the Fourier-Bessel series of $\tilde{G}$ in Theorem 1.8. Finally, Theorem 1.6 follows by combining Theorem 1.8 with the estimation (1.3.2) and using Definition 1.2.

For any $n \in \mathbb{N}^*$, we define extensions $\tilde{G}_n$ of $G$ by

$$\tilde{G}_n = \begin{cases} r^{2n} \sum_{k=0}^{2n} \dfrac{a_{k,n}}{k!} (r-a)^k & \text{if } r \leq a, \\ G(r) & \text{otherwise,} \end{cases} \tag{1.4.1}$$

where the values $a_{k,n}$ are chosen so that $\tilde{G}_n$ has continuous derivatives up to order $2n$:

$$a_{k,n} = \frac{d^k}{dr^k} \left( \frac{\log(r)}{r^{2n}} \right) \bigg|_{r=a}.$$

Observe that the $r^{2n}$ term ensures the boundedness of $(-\Delta)^n \tilde{G}_n$ near the origin. Moreover, since $\tilde{G}_n \equiv G$ in the neighborhood of $\partial B$, we have $(-\Delta)^s \tilde{G}_n = 0$ on $\partial B$ for any $s \in \mathbb{N}$.

**Lemma 1.7.** *There exists a constant $C$ independent of $n$ and $a$ such that for $r \leq a$*

$$\left| \Delta^n \tilde{G}_n(r) \right| \leq C \left( \frac{16n}{e} \right)^{2n} \max_{k \in \{1,\cdots,2n\}} \left( \frac{|a_{k,n}|}{k!} a^k \right). \tag{1.4.2}$$

*Proof.* For $r \leq a$, we have

$$|(-\Delta)^n \tilde{G}_n(r)| \leq \sum_{k=0}^{2n} \sum_{l=0}^{k} \binom{k}{l} \frac{|a_{k,n}|}{k!} a^{k-l} (2n+l)^2 (2(n-1)+l)^2 \times \ldots \times (2+l)^2 r^l.$$

Thus

$$\begin{aligned} |(-\Delta)^n \tilde{G}_n(r)| &\leq (4n)^2 (4n-2)^2 \times \ldots \times (2n+2)^2 \\ &\quad \times \max_{k \in [\![0,2n]\!]} \left( \frac{|a_{k,n}|}{k!} a^k \right) \sum_{k=0}^{2n} \sum_{l=0}^{k} \binom{k}{l} a^{-l} r^l. \end{aligned}$$

Since $r \leq a$, the last sum is bounded by $\displaystyle\sum_{k=0}^{2n} 2^k = 2^{2n+1} - 1 < 2^{2n+1}$, while

$$(4n)^2 (4n-2)^2 \times \ldots \times (2n+2)^2 \sim 2 \left( \frac{8n}{e} \right)^{2n}$$

follows from Stirling formula. □ □

**Lemma 1.8.** *For any $P \in \mathbb{N}^*$ and $a \in (0,1)$, there exists a radial function $\tilde{G}$ which coincides with $G$ on $\mathscr{A}(a)$ satisfying:*

$$\left\| \tilde{G} - \sum_{p=1}^{P} c_p(\tilde{G}) e_p \right\|_{H_0^1(B)} \leq C\sqrt{P} \exp\left( -\frac{aP\pi}{32} \right),$$

*where $C$ is a positive constant independent of $P$ and $a$.*

*Proof.* Let $n \in \mathbb{N}^*$. By the Leibniz formula, one has

$$a_{k,n} = \frac{(-1)^k k!}{a^{2n+k}} \left( -\sum_{j=0}^{k-1} \frac{\binom{2n+j-1}{j}}{k-j} + \binom{2n+k-1}{k} \log(a) \right).$$

Combining the identity $\sum_{j=0}^{k-1} \binom{j+2n-1}{j} = \frac{k}{2n} \binom{k+2n-1}{k}$ and the estimate

$$\binom{2n+k-1}{k} \leq \binom{4n-1}{2n} = \frac{1}{2} \binom{4n}{2n} \leq \frac{4^{2n}}{2\sqrt{2\pi n}} \quad \text{for } k \in \{1, \cdots, 2n\},$$

one finds

$$\max_{0 \leq k \leq 2n} \left( \frac{|a_{k,n}|}{k!} a^k \right) \leq \left( \frac{4}{a} \right)^{2n} \frac{1}{2\sqrt{2\pi n}} \left( \log\left( \frac{e}{a} \right) \right). \tag{1.4.3}$$

We apply Theorem 1.7 to get

$$|(-\Delta)^n \tilde{G}_n(r)| \leq \frac{C}{\sqrt{n}} \left( \frac{16n}{e} \right)^{2n} \left( \frac{4}{a} \right)^{2n} \log\left( \frac{e}{a} \right).$$

Since $(-\Delta)^n \tilde{G}_n(x) = (-\Delta)^n G(x) = 0$ outside $B(0,a)$, we obtain

$$\left\| (-\Delta)^n \tilde{G}_n \right\|_{L^2(B)} \leq \frac{Ca^2}{\sqrt{n}} \log\left( \frac{e}{a} \right) \left( \frac{64n}{ae} \right)^{2n}.$$

The conclusion now follows from Theorem 1.4. □ □

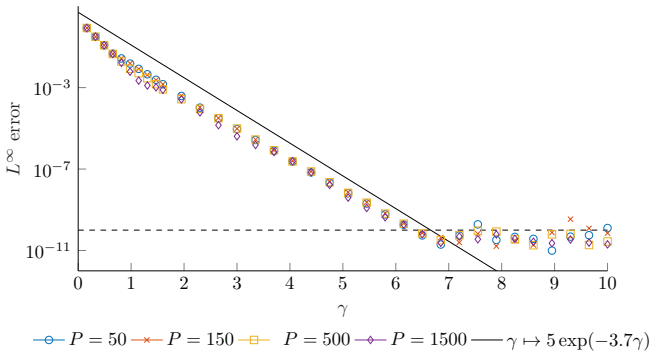


Figure 1.2: Evolution of the $L^\infty$ error over $[a,1]$ associated to the EBD for different values of $P$ in function of $\gamma$. An exponential decay is indeed observed at the roughly estimated rate of $\propto \exp(-3.7\gamma)$. The error stops decreasing at $e_{\min} \approx 10^{-10}$, for a value of $\gamma \approx 6.7$ because of the ill conditioning of the linear system (1.3.3)

*Remark* 1.3. We see that the convergence rate is bounded by a function of the parameter $\gamma = Pa$. Figure 1.2 displays the decay of the $L^\infty$ error with respect to $\gamma$ for different values of $P$. We observe that the error consistently decreases at an exponential rate of about $l_2 \approx 3.7$ and stagnates at the minimal error $e_{\min} \approx 10^{-10}$. We believe this stagnation is due to rounding errors related to the increasing condition number of the linear system (1.3.3).

### 1.4.2 Helmholtz kernel

Let $Y_0$ the classical Bessel function of second kind and of order 0. For any frequency number $k > 0$, the Helmholtz kernel, $r \mapsto \frac{-i}{4} H_0^{(1)}(kr)$, where $H_0^{(1)}(r) = J_0(r) + iY_0(r)$, is the Green kernel associated to the harmonic wave operator $-\Delta - k^2$, that satisfies a Sommerfeld radiation condition at infinity. This kernel arises in various physical problems such as sound waves scattering (see for example [27]). To approximate $H_0^{(1)}(kr)$ as a sum of dilated $J_0$ functions, it is sufficient to study the function of $r \mapsto Y_0(kr)$. We now have three different cases:

- **When $k$ is a root of $Y_0$**: In this case the multi-Dirichlet condition is satisfied at any order. Indeed, for any $n$,
$$(-\Delta)^n Y_0(kr)\big|_{r=1} = k^{2n} Y_0(k) = 0\,.$$
We thus compute the EBD decomposition of $Y_0$ on an interval $(a,1)$.

- **When $k$ is greater than the first root of $Y_0$**: we compute the EBD for $r \mapsto Y_0(k'r)$ on $(a,1)$, where $k'$ is the smallest root of $Y_0$ greater than $k$. This provides a decomposition for $r \mapsto Y_0(kr)$ valid on $(\frac{k'}{k}a, \frac{k'}{k})$.

- **When $k$ is much smaller than the first root of $Y_0$**: Here, instead of rescaling, one can use the Bessel-Fourier series associated to the Robin condition (see Section 1.2.3):
$$\frac{\partial u}{\partial n} + Hu = 0\,,$$
with $H = -\dfrac{kY_0'(k)}{Y_0(k)} > 0$ in this region.

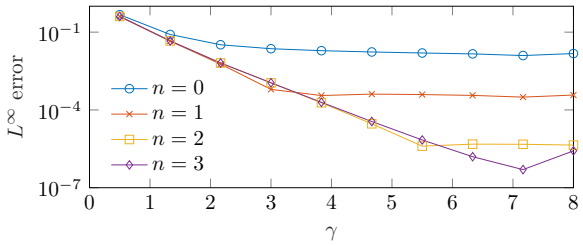


Figure 1.3: Maximal error between the kernel $G_1(r) = \log(x) + \sin(250x)$ and its 100-terms EBD in function of $\gamma = Pa$ using the method described in this paragraph for several values of $n$. Without any change to the method ($n = 0$) the $L^\infty$ error stops decreasing after some value of $\gamma$. Enforcing the multi-Dirichlet condition to higher order gradually improves the maximal reachable accuracy

### 1.4.3 General kernel : enforcing the multi-Dirichlet condition

For a general radial kernel $G$, the multi-Dirichlet conditions may not be fulfilled. When applying the EBD method without any changes, this leads to errors near $r = 1$. In this case, we apply the EBD to a modified function $H = G - K$ where $K$ is chosen to enforce the multi-Dirichlet condition. We can take for example

$$K(r) = \sum_{t=1}^{n} \mu_t J_0(\omega_t r),$$

where $\omega_1$ is the root of $J_1$ that is closest from the ratio $\sqrt{\left|\frac{G(1)}{\Delta G(1)}\right|}$ and $\omega_2, \cdots, \omega_n$, are the subsequent roots of $J_1$. The coefficients $(\mu_t)_{1\leq t\leq n}$ are found by solving

$$M\mu = \lambda,$$

where $\lambda$ is the vector given by

$$\lambda_t \quad = \quad (-\Delta)^t G\big|_{r=1}, \quad t \in \{1, \cdots, n\},$$

and

$$M = \begin{bmatrix} -\omega_1^2 & -\omega_2^2 & \cdots & -\omega_n^2 \\ \vdots & \vdots & \cdots & \vdots \\ (-1)^n \omega_1^{2n} & (-1)^n \omega_2^{2n} & \cdots & (-1)^n \omega_n^{2n} \end{bmatrix}.$$

In Figure 1.3, we show the efficiency of this method by applying the EBD with 100 terms to some highly oscillating function ($x \mapsto \log(x) + \sin(250x)$) and computing the maximal error of the decomposition in function of the parameter $\gamma = Pa$ (recall $P$ is the number of terms in the Bessel decomposition and $a$ is the inner radius of the annulus of approximation). We choose the frequencies $(\omega_t)_{1\leq t\leq n}$ as the roots of $J_1$ that are closest to 250. This figure illustrates the importance of the multi-Dirichlet condition for the fast decay of the error.

## 1.5 Circular quadrature

In this section, we study the approximation

$$J_0(\rho_p |x|) \approx \frac{1}{M_p} \sum_{m=0}^{M_p - 1} e^{i\rho_p \xi_m^p \cdot x},$$

where $M_p$ is an integer and with

$$\xi_m^p = \left(\cos\left(\frac{2m\pi}{M_p}\right), \sin\left(\frac{2m\pi}{M_p}\right)\right), \quad 0 \le m \le M_p - 1\,. \tag{1.5.1}$$

This approximation is obtained by applying the trapezoidal rule to the identity

$$J_0(|x|) = \int_{\partial B} e^{ix\cdot\xi} d\xi\,.$$

*Remark* 1.4. In the SCSD method, the Bessel functions are replaced by cardinal sines because

$$\mathrm{sinc}(|x|) = \frac{1}{4\pi}\int_{|\xi|=1} e^{ix\cdot\xi} d\sigma(\xi)\,,$$

where the integral is now taken over $\mathbb{S}^2 \subset \mathbb{R}^3$.

**Theorem 1.9.** *There exists a constant $K$ such that for any $r > 0$, for any integer $M \ge \frac{e}{2}r$, and for any $\varphi \in \mathbb{R}$*

$$\left| J_0(r) - \frac{1}{M}\sum_{m=0}^{M-1} e^{ir\sin\left(\frac{2m\pi}{M}-\varphi\right)} \right| \le K\left(\frac{er}{2M}\right)^M.$$

*Proof.* Let $f : x \mapsto e^{ir\sin(x-\varphi)}$. For any $k \in \mathbb{Z}$, one has

$$J_k(r) = \int_0^{2\pi} e^{ir\sin(x)} e^{-ikx} dx = e^{-ik\varphi}\int_0^{2\pi} f(x) e^{-ikx} dx\,.$$

Thus, the (usual) Fourier coefficient of $f$ are given by

$$c_k(f) = e^{ik\varphi} J_k(r).$$

Consequently, the aliasing formula yields

$$J_0(r) - \frac{1}{M}\sum_{j=0}^{M-1} e^{ir\sin\left(\frac{2j\pi}{M}-\varphi\right)} = -\sum_{k\in\mathbb{Z}^*} e^{iNk\varphi} J_{Nk}(r)\,.$$

For large $|k|$, we have

$$J_k(r) \sim \left(\frac{er}{2\,|k|}\right)^{|k|}.$$

Therefore, there exists a constant $C'$ such that:

$$\begin{aligned}\left| J_0(r) - \frac{1}{M}\sum_{m=0}^{M-1} e^{ir\sin\left(\frac{2m\pi}{M}-\varphi\right)} \right| &\le C' \sum_{k\in\mathbb{Z}^*} \left(\frac{er}{2M|k|}\right)^{M|k|} \\ &\le K\left(\frac{er}{2M}\right)^M\end{aligned}$$

for an appropriate choice of $K$. □ □

We conclude with the following result

**Proposition 1.10.** *Let $\varepsilon > 0$, $r > 0$, and assume $M > \frac{e}{2} r + \log\left(\frac{K}{\varepsilon}\right)$. Then*

$$\left| J_0(r) - \frac{1}{M} \sum_{m=0}^{M-1} e^{ir\sin\left(\frac{2m\pi}{M} - \varphi\right)} \right| \leq \varepsilon \,.$$

*Proof.* This results from Theorem 1.9 and the following inequality:

$$\forall (A,B) \in \left(\mathbb{R}_+^*\right)^2, \quad \left(\frac{A}{A+B}\right)^{A+B} \leq e^{-B} \,.$$

which may be proved using $\left(1+x^{-1}\right)\log(1+x) \geq 1$ valid for all $x \neq 0$. □ □

Our numerical tests suggest that the constant $\frac{e}{2}$ in the previous estimation is sharp.

## 1.6 Proof of the complexity

We now sum up all the results obtained in the previous sections to prove the complexity of the complete algorithm given in Section 1.1. We fix a free parameter $\eta \in [0, 1/6]$ and choose the inner radius of the annulus of approximation as

$$a = \frac{1}{N_z^{2/3-\eta}} \,. \tag{1.6.1}$$

We give a bound for the number of operations in function of the number of nodes $N_z$, the target tolerance $\varepsilon$ and $\eta$. Let $C_{\text{EBD}}$, $C_{\text{circ}}$, $C_{\text{assemble}}$, $C_{\text{far}}$ and $C_{\text{close}}$ respectively denote the number of operations required to compute the EBD, the circular quadrature, to assemble the close correction matrix $D$ (1.1.3), to compute the far approximation (1.1.4), and to apply $D$ on a vector. In the sequel, $C$ is used for any positive constant that is independent of $N_z$, $\varepsilon$ and $\eta$.

### 1.6.1 Offline computations

**1.6.1.a Trigonometric representation** Recall that we compute a trigonometric representation of the form (1.2) for the kernel $G(r) = \log(r)$, by first computing its EBD:

$$G(x) \approx \sum_{p=1}^{P} \alpha_p e_p(x) \,,$$

where $e_p(r) = C_p J_0(\rho_p r)$ are the normalized eigenfunctions of the Laplace operator and the number of terms $P$ is chosen large enough so that the $L^\infty$ error is below the required tolerance. In a second step, each function $e_p$ is replaced by the circular quadrature analyzed in Section 1.5.

**Efficient Bessel Decomposition.** If the EBD is applied on the annulus $\{a < r < 1\}$, Theorem 1.6 shows that the tolerance $\frac{\varepsilon}{2}$ is reached for

$$P = O\left(\frac{|\log(\varepsilon)|}{a}\right) . \tag{1.6.2}$$

Since the coefficients are obtained through the inversion of a $P \times P$ matrix, the computation of the EBD requires $O(P^3)$ computations. Therefore, with $a$ defined as in (1.6.1), one has

$$C_{\text{EBD}}(N_z, \varepsilon, \eta) \leq C \left|\log \varepsilon\right|^3 N_z^{2-3\eta} \,. \tag{1.6.3}$$

**Circular quadrature.** Using the notation of Section 1.5, we choose the number $M_p$ of terms in the circular quadrature for each $e_p$ such that

$$\left| e_p(|x|) - \frac{C_p}{M_p} \sum_{m=1}^{M_p} e^{i\rho_p x \cdot \xi_m^p} \right| \leq \frac{\varepsilon}{2P|\alpha_p|} \quad a < |x| < 1\,. \tag{1.6.4}$$

By the triangle inequality, this ensures that the maximal error in the trigonometric representation of $G$ is less than $\varepsilon$. According to Theorem 1.10, we may choose $M_p$ such that

$$M_p > \frac{e}{2}\rho_p + \log\left(\frac{2KP|\alpha_p|C_p}{\varepsilon}\right). \tag{1.6.5}$$

Bessel's identity ensures the boundedness of $\alpha_p$, and the constants $C_p$ are bounded by estimation (1.2.2). Since $\rho_p = O(p)$, the total number of terms $N_\xi$ in the trigonometric representation is of the order

$$N_\xi = \sum_{p=1}^{P} M_p = O(P^2) \tag{1.6.6}$$

and $C_{\text{circ}}(N_z, \varepsilon, \eta) \leq C|\log\varepsilon|^2 N_z^{4/3-2\eta}$. We thus see that the EBD dominates the complexity for computing the trigonometric representation, and the estimation (1.6.3) yields the first part of Theorem 1.1.

**1.6.1.b Close correction matrix:** Recall that $\delta_{\max}$ is the diameter of the cloud of nodes $(z_k)$. Fix $\delta_{\min} := a\delta_{\max}$. We first determine the set $\mathscr{P}$ of all pairs $(k,l)$ such that $|z_k - z_l| \leq \delta_{\min}$. This is the classical "fixed-radius near neighbors search", and can be solved in $O(N_z \log N_z + \#\mathscr{P})$ operations (see for example [6, 7, 11, 25]). In order to compute the close correction sparse matrix:

$$D_{kl} = \delta_{(k,l)\in\mathscr{P}} \left( G(z_k - z_l) - \sum_{p=1}^{P} \alpha_p J_0\left(\frac{\rho_p}{\delta_{\max}}|z_k - z_l|\right)\right),$$

we need $\#\mathscr{P}$ evaluations of log. For the computation of the second term, we use a piecewise polynomial interpolation of the smooth function.

$$f : r \mapsto \sum_{p=1}^{P} \alpha_p J_0(\rho_p r)\,, \quad r \in (0,a)\,.$$

This involves only a small number of interpolation nodes, and the sum can be evaluated in $O(N_z)$ operations. For a set of nodes uniformly distributed on a curve, we have

$$\#\mathscr{P} = O\left(\frac{\delta_{\min}}{\delta_{\max}} N_z\right) = O(N_z^2 a)\,. \tag{1.6.7}$$

We thus get

$$C_{\text{close}}(N_z, \varepsilon, \eta) \leq C N_z^{4/3+\eta}\,. \tag{1.6.8}$$

This is the second part of Theorem 1.1.

### 1.6.2 Online Computations

**Far approximation.** Recall that for all $k \in \{1, \cdots, N_z\}$, the far approximation is defined by the following equation:

$$q_k^{\text{far}} = \sum_{l=1}^{N_z} G_{\text{trig}}(z_k - z_l) f_l,$$

where

$$G_{\text{trig}}(x) = \sum_{\nu=1}^{N_\xi} \hat{\omega}_\nu e^{ix\cdot\xi_\nu}.$$

To compute $q^{\text{far}}$, recall the following three steps:

(i) **Space $\to$ Fourier:** Compute $\hat{f} = \text{NUFFT}_-[z, \xi](f)$,

(ii) **Fourier multiply** Perform element wise multiplication by $\hat{\omega}$:

$$\hat{g}_\nu = \hat{\omega}_\nu \hat{f}_\nu,$$

(iii) **Fourier $\to$ Space:** Compute $q^{\text{far}} = \text{NUFFT}_+[z, \xi](\hat{g})$.

According to [16, Sec. 4.3], the complexity of the NUFFT of type 3 is

$$O\left(B_1 B_2 \log(B_1 B_2) + |\log \varepsilon|^2 (N_x + N_\xi)\right)$$

where $B_1$ and $B_2$ are the bandwidth parameters along each dimension. Here all frequencies lie in a circle of radius $\rho_P = O(P)$, thus $B_1 B_2 = O(P^2)$. On the other hand, equations (1.6.1) and (1.6.6) imply that $N_\xi \geq N_z$, and by (1.6.6), $N_\xi = O(P^2)$. Therefore, the complexity of the NUFFT is $O(P^2 \log(P) |\log \varepsilon|^2)$. By definition (1.6.1) and eq. (1.6.2), we conclude

$$C_{\text{far}}(N_z, \varepsilon, \eta) \leq C N_z^{4/3-2\eta} \log(N_z) |\log \varepsilon|^4. \tag{1.6.9}$$

**Close correction.** Since $D$ has $\#\mathscr{P}$ non-zero entries, we get

$$C_{\text{close}}(N_z, \varepsilon, \eta) \leq C N_z^{4/3+\eta}. \tag{1.6.10}$$

Summing (1.6.9) and (1.6.10) yields the second part of Theorem 1.1.

*Remark* 1.5. The extreme cases $\eta = 0$ and $\eta = 1/6$ correspond respectively to the situations where one wishes to either minimize the total (offline + online) computation time or just the online time. The corresponding complexities are given in the table below (omitting the dependence in $\varepsilon$):

| | $\eta = 0$ | $\eta = 1/6$ |
|---|---|---|
| Offline | $O(N_z^2)$ | $O\left(N_z^{3/2} \log N_z\right)$ |
| Online | $O(N_z^{4/3} \log(N_z))$ | $O(N_z^{3/2})$ |

Table 1.1: Complexity of the algorithm (omitting dependence in $\varepsilon$) in the two extreme cases $\eta = 0$ and $\eta = 1/6$.

## 1.7 Performance of the method and comparison with *Fastsum*

In this section, we apply our method (which we call EBD) to compute the vector $q$ given by

$$q_k = \sum_{l=1}^{N} G(X_k - Y_l) f_l, \quad k = 1, \cdots, N$$

where $X$ and $Y$ are two distinct clouds of points in $\mathbb{R}^2$ of size $N$. The performance is compared with *Fastsum*, which sources are downloaded from the toolbox [1]. We study three kernels, $G_1(x) = \log(x)$, $G_2(x) = x^2 \log(x)$ and $G_3(x) = \frac{1}{x^2}$. We measure the computing times for $N$ from $10^3$ to $10^6$. The computer used for these tests is a laptop cadenced to 1.6 GHz and possessing 4GB of memory.

We measure the "offline" time as the time needed to set up the method and compute the first discrete convolution. The "online" time is the average time needed for the subsequent convolutions.

**Parameter setting.** For *Fastsum*, we use the parameter setting described in [20] for singular kernels. For the first two kernels, we use the cut-off parameter $m = 4$ and the degree of regularization $p = 3$. The approximate error level $\varepsilon$ is measured by computing the maximal absolute error between $G(X_1 - Y_l)$ and its approximation by the trigonometric polynomial for $l = 1, \cdots, N$. This is taken as the (input) target tolerance in the EBD. For the third kernel, it is necessary to increase $m$ and $p$ in *Fastsum* to obtain an acceptable error. In such case, we take $p = m$ and choose the first value for which the error goes below 1. In our algorithm, the only free parameter is the inner radius of the annulus of approximation $\delta_{\min}$. Depending on the case, we set $\delta_{\min} = \frac{\lambda}{\sqrt{N}} \delta_{\max}$ with $\lambda$ ranging from 2 to 20.

**Programming language.** Our program is written in Matlab except for the NUFFT routine which is the FORTRAN routine borrowed from the NYU website [2]. In contrast, Fastsum is fully written in C. This difference only plays a role in the offline computations, since in the online stage, most of the time is spent in the NUFFT for both methods.

**Discussion.** We observe that our method yields a representation of the radial kernel with much less frequency samples (a factor 100 is observed in most cases). The offline computations for EBD are always longer (by a factor 2 to 4 in computational intensive cases). After that, our method is faster than *Fastsum* for evaluating the convolution in every case, in general by a factor 2 to 3. This gain in online performance for EBD is particularly useful when one wishes to solve iteratively a large linear system with matrix entries of the form $G(X_k - Y_l)$.

In our algorithm, the 1D approximation allows for an accurate estimation of the error which can therefore be given and controlled as an input. Instead, in *Fastsum*, the parameters need a fine tuning "by hand" in order to achieve a given accuracy.

On the other hand, there is a free parameter in the EBD method, $\delta_{\min}$, that determines the performance. When the distribution of the nodes is known, the above analysis provides a way to select $\delta_{\min}$ to ensure a quasi-linear complexity. However, it is not clear how to choose the optimal value for $\delta_{\min}$ automatically when the distribution of nodes is not known.

Table 1.3: Computing times (s) for the kernel $G(x) = x^2 \log(x)$

| | *Fastsum* | | | | EBD | | | |
|---|---|---|---|---|---|---|---|---|
| $N$ | $N_\xi$ | Offline | Online | $\varepsilon$ | $N_\xi$ | Offline | Online | $\varepsilon$ |
| $10^3$ | 1.3e4 | 2.2e-2 | 5.9e-3 | 1e-5 | 166 | 0.92 | 2.6e-3 | 6.3e-6 |
| $10^4$ | 1.2e5 | 0.15 | 7.4e-2 | 7.6e-7 | 1.7e3 | 0.94 | 2.5e-2 | 5.3e-7 |
| $10^5$ | 1.2e6 | 1.5 | 0.91 | 2.1e-8 | 3.2e4 | 3.8 | 0.35 | 2e-8 |
| $10^6$ | 1.2e7 | 16 | 10 | 1.5e8 | 3.7e5 | 28 | 8 | 1.5e8 |

Table 1.4: Computing times (s) for the kernel $G(x) = \frac{1}{x^2}$

| | *Fastsum* | | | | EBD | | | |
|---|---|---|---|---|---|---|---|---|
| $N$ | $N_\xi$ | Offline | Online | $\varepsilon$ | $N_\xi$ | Offline | Online | $\varepsilon$ |
| $10^3$ | 2.1e4 | 2.5e-2 | 7e-3 | 6e-2 | 1.5e2 | 0.45 | 1.8e-3 | 5e-2 |
| $10^4$ | 2.4e5 | 0.23 | 0.12 | 0.17 | 5.2e3 | 1.2 | 1.65e-2 | 0.14 |
| $10^5$ | 2.8e6 | 3 | 1.5 | 0.2 | 1.5e5 | 7.8 | 0.36 | 0.2 |
| $10^6$ | 3.2e7 | 45 | 25 | 0.6 | 5.2e6 | 145 | 16.5 | 0.5 |

Table 1.2: Computing times (s) for the kernel $G(x) = \log(x)$

| | *Fastsum* | | | | EBD | | | |
|---|---|---|---|---|---|---|---|---|
| $N$ | $N_\xi$ | Offline | Online | $\varepsilon$ | $N_\xi$ | Offline | Online | $\varepsilon$ |
| $10^3$ | 1.2e4 | 2.1e-2 | 5.7e-3 | 1.3e-3 | 150 | 0.31 | 2.0e-3 | 1e-3 |
| $10^4$ | 1.2e5 | 0.14 | 7.3e-2 | 1.3e-3 | 2.4e3 | 0.7 | 1.3e-2 | 1.2e-3 |
| $10^5$ | 1.2e6 | 1.4 | 0.9 | 1.3e-3 | 2.8e4 | 3.8 | 0.15 | 1.2e-3 |
| $10^6$ | 1.2e7 | 16 | 10 | 1.3e-3 | 1.2e6 | 30 | 4.6 | 1.3e-3 |

## Conclusion

The method that we have presented (EBD) generalizes the SCSD method of [4] from 3 to 2 dimensions. Compared to SCSD, the cardinal sines must be replaced by Bessel functions, and the Fourier series appearing in 3D become Fourier-Bessel series in 2D. We have provided a complete analysis of the complexity and the error of our method. It is shown that the computational complexity is quasi-linear in terms of the number of nodes. We also provide numerical results that confirm the theoretical estimations. It has appeared that the structure of SCSD and EBD is very similar to that of *Fastsum*, differing only by the choice of the frequency samples. By exploiting the radial symmetry, our method allows to reduce drastically the number of those samples. As a result, after some precomputations, the EBD yields faster approximations of the discrete convolutions than *Fastsum*. Future work includes generalizing the present approach to $n$ dimensions, and the automatic fine-tuning of the remaining free parameter of the method, $\delta_{\min}$.

# Bibliography

[1] NFFT project. See `https://www-user.tu-chemnitz.de/~potts/nfft/download.php`.

[2] NUFFT package. See `https://cims.nyu.edu/cmcl/nufft/nufft.html`.

[3] M. Abramowitz and I. A. Stegun. *Handbook of mathematical functions: with formulas, graphs, and mathematical tables*, volume 55. Courier Corporation, 1964.

[4] F. Alouges and M. Aussal. The sparse cardinal sine decomposition and its application for fast numerical convolution. *Numerical Algorithms*, 70(2):427–448, 2015.

[5] M. Averseng. EBD toolbox. See `https://github.com/MartinAverseng/EBD`.

[6] J. L. Bentley. Multidimensional binary search trees used for associative searching. *Communications of the ACM*, 18(9):509–517, 1975.

[7] J. L. Bentley, D. F. Stanat, and E. H. Williams. The complexity of finding fixed-radius near neighbors. *Information processing letters*, 6(6):209–212, 1977.

[8] H. Cheng, L. Greengard, and V. Rokhlin. A fast adaptive multipole algorithm in three dimensions. *Journal of computational physics*, 155(2):468–498, 1999.

[9] R. Coifman, V. Rokhlin, and S. Wandzura. The fast multipole method for the wave equation: A pedestrian prescription. *IEEE Antennas and Propagation Magazine*, 35(3):7–12, 1993.

[10] J. W. Cooley and J. W. Tukey. An algorithm for the machine calculation of complex fourier series. *Mathematics of computation*, 19(90):297–301, 1965.

[11] M. T. Dickerson and R. S. Drysdale. Fixed-radius near neighbors search algorithms for points and segments. *Information Processing Letters*, 35(5):269–273, 1990.

[12] A. Dutt and V. Rokhlin. Fast fourier transforms for nonequispaced data. *SIAM J. Sci. Comput.*, 14(6):1368–1393, November 1993.

[13] D. S Grebenkov and B-T Nguyen. Geometrical structure of laplacian eigenfunctions. *SIAM Review*, 55(4):601–667, 2013.

[14] L. Greengard. *The rapid evaluation of potential fields in particle systems*. MIT press, 1988.

[15] L. Greengard and J. Y. Lee. Accelerating the nonuniform fast fourier transform. *SIAM review*, 46(3):443–454, 2004.

[16] J. Keiner, S. Kunis, and D. Potts. Using nfft 3—a software library for various nonequispaced fast fourier transforms. *ACM Transactions on Mathematical Software (TOMS)*, 36(4):19, 2009.

[17] June-Yub Lee and Leslie Greengard. The type 3 nonuniform fft and its applications. *Journal of Computational Physics*, 206(1):1–5, 2005.

[18] F. W. J. Olver, A. B. Olde Daalhuis, D. W. Lozier, B. I. Schneider, R. F. Boisvert, C. W. Clark, B. R. Miller, and B. V. Saunders. *NIST Digital Library of Mathematical Functions*. http://dlmf.nist.gov/, Release 1.0.16 of 2017-09-18.

[19] D. Potts, G. Pöplau, , and U. van Rienen. Calculation of 3d space-charge fields of bunches of charged particles by fast summation. In *Scientific Computing in Electrical Engineering*, volume 11, pages 241–246. Springer, 2006.

[20] D. Potts, G. Steidl, and A. Nieslony. Fast convolution with radial kernels at nonequispaced knots. *Numerische Mathematik*, 98(2):329–351, 2004.

[21] D. Potts, G. Steidl, and M. Tasche. Fast fourier transforms for nonequispaced data: A tutorial. In *Modern sampling theory*, pages 247–270. Springer, 2001.

[22] V. Rokhlin. Rapid solution of integral equations of scattering theory in two dimensions. *Journal of Computational Physics*, 86(2):414–439, 1990.

[23] V. Rokhlin. Diagonal forms of translation operators for the helmholtz equation in three dimensions. *Applied and Computational Harmonic Analysis*, 1(1):82–93, 1993.

[24] G. P. Tolstov. *Fourier series*. Courier Corporation, 2012.

[25] V. Turau. Fixed-radius near neighbors search. *Information processing letters*, 39(4):201–203, 1991.

[26] G. N. Watson. *A treatise on the theory of Bessel functions*. Cambridge university press, 1995.

[27] C. H. Wilcox. *Scattering theory for the d'Alembert equation in exterior domains*, volume 4. Springer Berlin, 1975.

# Chapter 2

# Laplace and Helmholtz equations on open curves

## Part I: Analytical Framework and Numerical results

Fusionner avec la version longue.

**Abstract:** Studying wave scattering problems in 2D by open arcs leads to ill-conditioned systems. This is partly due to the singular behavior of the solutions near the edges of the arc. We introduce two new preconditioners to tackle this problem either with Dirichlet or Neumann boundary data, that take the form of square roots of local operators. We introduce an adapted analytical setting to analyze them and demonstrate the efficiency of this method on several numerical examples. A complete suitable pseudo-differential calculus for the complete study of such operators is postponed to the second part of this work.

## 2.1 Introduction

The problem of preconditionning the linear systems coming from the discretization of first kind integral equations has received considerable attention since two decades. Among the possible strategies are the so-called pseudo-differential preconditionners [3, 4, 5, 11, 15, 38]. Roughly speaking, if the original problem is written in the abstract form

$$\mathscr{L}u = f\,, \tag{2.1.1}$$

where $\mathscr{L}$ is a linear operator, the strategy consists in left multiplying equation (2.1.1) by an operator $\mathscr{K}$ and solve

$$\mathscr{K}\mathscr{L}u = \mathscr{K}f\,. \tag{2.1.2}$$

Now, if $\mathscr{K}\mathscr{L}$ is a compact perturbation of the identity, the condition number of the discretized underlying linear system becomes independent of the mesh size, enabling the efficient use of iterative methods such as GMRES [31]. This is in particular the case when $\mathscr{K}$ is a parametrix of $\mathscr{L}$, which is usually proven using tools from pseudo-differential calculus [36].

Several strategies, depending on the problem to solve (e.g. Helmholtz or Maxwell equations) have been studied in the literature to propose such operators $\mathscr{K}$, that often turn out to be very effective in practice, when numerical applications are considered. Among those, we would like to emphasize the viewpoint first proposed in [3, 4], where, for Helmholtz equation, the authors consider integral formulations of the problem that involve the Dirichlet-Neumann map *DN* which leads to well-conditioned systems after discretization. Combined with the approximation of *DN* proposed first in [5] under the form of the square root operator

$$DN \sim \sqrt{-\Delta_\Gamma - k^2}\,, \tag{2.1.3}$$

where $\Delta_\Gamma$ stands for the Laplacian operator on the surface $\Gamma$, the method (called GCSIE) yields a very impressive reduction of the number of iterations.

However, all the preceding results and theories are limited to smooth surfaces $\Gamma$ and very little is known when the integral equation is posed on non-smooth domains, such as domains with corners (in 2D), wedges or conical points (in 3D). One of the reasons might be the fact that pseudo-differential calculus is difficult to generalize on such manifolds and the existing theories such as the ones presented in e.g. [24, 33, 34] do not seem to be adequate for the analysis of such problems.

Nevertheless, attempts to precondition the integral equations that come from the discretization of single-layer or double-layer potentials for Laplace equation on singular domains has started a few years ago [10, 15, 16, 17, 30] in dimension 2 or 3, but for very particular domains such as a straight and then curved segments in 2D and a unit disc in 3D. In most of these works, weighted versions of the usual integral operators are introduced, which enjoy better mapping properties than the standard operators, and the analysis is obtained "by hand" without any explicit use of pseudo-differential calculus.

The aim of this paper and the forthcoming [7] is twofold. Here we describe an analytical framework and a Galerkin method suited to the inversion of these weighted operators, with optimal rates of convergence. On the other hand, we build efficient preconditioners for the linear systems arising from the previous Galerkin method. The complete description and analysis of the method is postponed to [7] and we instead focus in the present paper on the description and the numerical implementation. Preliminary analytical results, that show the optimality of the approach for Laplace problems, are nevertheless included here.

The paper is organized as follows: in the first section, we introduce the notations and the usual boundary integral operators on an open curve. In the second section, we treat the case of the Laplace equation, where it is possible to derive explicit inverses of the weighted layer potentials in terms of square roots of local operators. We then generalize our results to non-zero frequency and non-flat arc in the third section. In the last section, we show the efficiency of this approach on several numerical examples.

## 2.2 The scattering problem outside an open curve

Let $\Gamma$ be a smooth non-intersecting bounded open curve in $\mathbb{R}^2$, and let $k \geq 0$ the wave number. We seek a solution of the Helmholtz equation

$$-\Delta u - k^2 u = 0, \text{ in } \mathbb{R}^2 \setminus \Gamma \tag{2.2.1}$$

when one considers furthermore Dirichlet or Neumann boundary conditions, namely

$$u = u_D, \text{ on } \Gamma \tag{2.2.2}$$

or

$$\frac{\partial u}{\partial n} = u_N \text{ on } \Gamma \tag{2.2.3}$$

respectively. In order for the problem to be well posed, we also need to impose suitable decay at infinity, given by the Sommerfeld condition

$$\frac{\partial u}{\partial r} - iku = o\left(\frac{1}{\sqrt{r}}\right) \tag{2.2.4}$$

with $r = |x|$ for $x \in \mathbb{R}^2$ . Notice that in equation (2.2.3), $n$ stands for a smooth unit vector normal to $\Gamma$. Existence and uniqueness of solutions to the previous problems are guaranteed by the following theorem.

**Theorem 2.1.** *[25, 37, 39]. Assume $u_D \in H^{1/2}(\Gamma)$, and $u_N \in H^{-1/2}(\Gamma)$. Then problems (2.2.1,2.2.2,2.2.4) and (2.2.1,2.2.3,2.2.4) both possess a unique solution $u \in H^1_{\text{loc}}(\mathbb{R}^2 \setminus \Gamma)$, which is of class $C^\infty$ outside $\Gamma$.*

For the definition of Sobolev spaces on smooth open curves, we follow [22] by considering any smooth closed curve $\tilde{\Gamma}$ containing $\Gamma$, and defining

$$H^s(\Gamma) = \left\{ U_{|\Gamma} \;\middle|\; U \in H^s(\tilde{\Gamma}) \right\}.$$

This definition does not depend on the particular choice of the closed curve $\tilde{\Gamma}$ containing $\Gamma$. Moreover, we also define

$$\tilde{H}^s(\Gamma) = \left\{ u \in H^s(\Gamma) \;\middle|\; \tilde{u} \in H^s(\tilde{\Gamma}) \right\}$$

where $\tilde{u}$ denotes the extension by zero of $u$ on $\tilde{\Gamma}$.

The solution to (2.2.1,2.2.2,2.2.4) and (2.2.1,2.2.3,2.2.4) can be furthermore expressed in terms of the Green function associated to the problem

$$\begin{cases} G_0(z) = -\dfrac{1}{2\pi} \ln|z|, & \text{if } k = 0, \\ G_k(z) = \dfrac{i}{4} H_0(k|z|), & \text{if } k > 0, \end{cases} \tag{2.2.5}$$

where $H_0$ is the Hankel function of the first kind. The expressions involve the so-called single-layer, double-layer and hypersingular potentials that we recall now. The single-layer potential is defined by

$$\forall x \notin \Gamma, \quad \mathscr{S}_k \lambda(x) = \int_\Gamma G_k(x-y)\lambda(y) d\sigma_y \tag{2.2.6}$$

and the solution $u$ of the Dirichlet problem (2.2.1,2.2.2,2.2.4) can be expressed as

$$u = \mathscr{S}_k \lambda \tag{2.2.7}$$

where $\lambda \in \tilde{H}^{-1/2}(\Gamma)$ is the unique solution to

$$S_k \lambda = u_D. \tag{2.2.8}$$

Here, the operator $S_k$ is defined by $S_k := \gamma\mathscr{S}_k$, where $\gamma$ is the trace operator on $\Gamma$. The operator $S_k$ maps continuously $\tilde{H}^{-1/2}(\Gamma)$ to $H^{1/2}(\Gamma)$ [39, Theorem 1.8]. Similarly, we introduce the double layer potential $\mathscr{D}_k$ by

$$\mathscr{D}_k\mu(x) = \int_\Gamma n(y)\cdot\nabla G_k(x-y)\mu(y)d\sigma_y$$

for any smooth function $\mu$ defined on $\gamma$. The normal derivative of $\mathscr{D}_k\mu$ is continuous across $\Gamma$, allowing us to define the hypersingular operator $N_k = \partial_n\mathscr{D}_k$. This latter operator admits the representation for $x\in\Gamma$

$$(N_k\mu)(x) = \lim_{\varepsilon\to 0^+}\int_\Gamma n(y)\cdot\nabla G_k(x+\varepsilon n(x)-y)\mu(y)d\sigma_y. \tag{2.2.9}$$

The kernel of this operator has a non-integrable singularity, but numerical calculations are made possible by the following formula, valid for smooth functions $\mu$ and $\nu$ that vanish at the extremities of $\Gamma$:

$$\begin{aligned}\langle N_k\mu,\nu\rangle \;=\; &\int_{\Gamma\times\Gamma} G_k(x-y)\mu'(x)\nu'(y)\\ &-k^2G_k(x,y)\mu(x)\nu(y)n(x)\cdot n(y)d\sigma_x d\sigma_y\,.\end{aligned} \tag{2.2.10}$$

It is also known that $N_k$ maps $\tilde{H}^{1/2}(\Gamma)$ to $H^{-1/2}(\Gamma)$ continuously [39, Theorem 1.4], and that the solution $u$ to the Neumann problem (2.2.1,2.2.3,2.2.4) can be written as

$$u = \mathscr{D}_k\mu \tag{2.2.11}$$

where $\mu\in\tilde{H}^{1/2}(\Gamma)$ solves

$$N_k\mu = u_N\,. \tag{2.2.12}$$

It is also known that $\lambda$ and $\mu$ are singular singular near the edges of the arc $\Gamma$ their respective asymptotics are given by the following proposition.

**Proposition 2.2.** *[25, 37, 39]. Near the edges of the arc $\Gamma$, $\lambda$ is unbounded:*

$$\lambda(x) = O\left(\frac{1}{\sqrt{d(x,\partial\Gamma)}}\right),$$

*while $\mu$ is locally given by*

$$\mu(x) = C\sqrt{d(x,\partial\Gamma)}+\psi.$$

*where $\psi\in\tilde{H}^{3/2}(\Gamma)$ and $C$ is a constant.*

In both cases (Dirichlet or Neumann problems) numerical approximations of the solution can be sought by a suitable discretization of the equations (2.2.8) and (2.2.12) respectively. This amounts to solve linear systems which turn out to be ill-conditioned in practice, and the aim of the paper is to provide the reader with a formalism that enables to give preconditioned version of them.

## 2.3 Laplace equation on a flat segment

We first restrict our attention to the case where $\Gamma$ is the segment

$$\Gamma = [-1,1]\times\{0\},$$

and the wavenumber $k = 0$, by considering the equations

$$S_0\lambda = u_D \quad \text{and} \quad N_0\mu = u_N\,.$$

These problems have been already considered thoroughly in the literature, both in terms of analytical and numerical properties (see for instance [10, 18]). However, to the best of our knowledge, the natural inverses in terms of square roots of local operators have remained unnoticed. In order to derive suitable preconditonners for such equations and their corresponding expressions, we need to introduce the following analytical setting. As it is well known, Chebyshev polynomials of first and second kind play an important role.

### 2.3.1 Analytical setting

We introduce the Chebyshev polynomials of first and second kinds [21], respectively given by

$$T_n(x) = \cos(n\arccos(x)),$$

and

$$U_n(x) = \frac{\sin((n+1)\arccos(x))}{\sqrt{1-x^2}}\,,$$

and we call $\omega$ the operator $\omega : u(x) \mapsto \omega(x)u(x)$ with $\omega(x) = \sqrt{1-x^2}$. We also denote by $\partial_x$ the derivation operator. The Chebyshev polynomials satisfy the ordinary differential equations

$$(1-x^2)\partial_{xx}T_n - x\partial_x T_n + n^2 T_n = 0$$

and

$$(1-x^2)\partial_{xx}U_n - 3x\partial_x U_n + n(n+2)U_n = 0$$

which can be rewritten under the form

$$(\omega\partial_x)^2 T_n = -n^2 T_n\,, \tag{2.3.1}$$

$$(\partial_x\omega)^2 U_n = -(n+1)^2 U_n\,. \tag{2.3.2}$$

(Notice that by $(\partial_x\omega)f$ we mean $\partial_x(\omega f)$.) Both $T_n$ and $U_n$ are polynomials of degree $n$, and form orthogonal families respectively of the Hilbert spaces

$$L^2_{\frac{1}{\omega}} := \left\{ u \in L^1_{\text{loc}}(-1,1) \;\middle|\; \int_{-1}^{1} \frac{f^2(x)}{\sqrt{1-x^2}}dx < +\infty \right\}$$

and

$$L^2_{\omega} := \left\{ u \in L^1_{\text{loc}}(-1,1) \;\middle|\; \int_{-1}^{1} f^2(x)\sqrt{1-x^2}dx < +\infty \right\}.$$

We denote by $(\cdot,\cdot)_{\frac{1}{\omega}}$ and $(\cdot,\cdot)_{\omega}$ the inner products of $L^2_{\frac{1}{\omega}}$ and $L^2_{\omega}$,

$$(u,v)_{\frac{1}{\omega}} := \frac{1}{\pi}\int_{-1}^{1} \frac{u(x)\overline{v(x)}}{\omega(x)}dx\,, \quad (u,v)_{\omega} := \frac{1}{\pi}\int_{-1}^{1} u(x)\overline{v(x)}\omega(x)dx\,.$$

The Chebyshev polynomials satisfy

$$(T_n,T_m)_{\frac{1}{\omega}} = \begin{cases} 0 \text{ if } n \neq m \\ 1 \text{ if } m = n = 0 \\ 1/2 \text{ otherwise} \end{cases} \tag{2.3.3}$$

and

$$(U_n, U_m)_\omega = \begin{cases} 0 \text{ if } n \neq m \\ 1/2 \text{ otherwise} \end{cases} \tag{2.3.4}$$

which provides us with the so-called Fourier-Chebyshev decomposition. Any $u \in L^2_{\frac{1}{\omega}}$ can be decomposed through the first kind Chebyshev series

$$u(x) = \sum_{n=0}^{+\infty} \hat{u}_n T_n(x) \tag{2.3.5}$$

where the Fourier-Chebyshev coefficients $\hat{u}_n$ are given by $\hat{u}_n := \dfrac{(u_n, T_n)_{\frac{1}{\omega}}}{(T_n, T_n)_{\frac{1}{\omega}}}$. Similarly, any function $v \in L^2_\omega$ can be decomposed along the $(U_n)_{n\geq 0}$ as

$$v(x) = \sum_{n=0}^{+\infty} \check{v}_n U_n(x)$$

where the coefficients $\check{v}_n$ are given by $\check{v}_n := \dfrac{(v, U_n)_\omega}{(U_n, U_n)_\omega}$. Those properties can be used to define Sobolev-like spaces.

**Definition 2.1.** For all $s \geq 0$, we define

$$T^s = \left\{ u \in L^2_{\frac{1}{\omega}} \;\middle|\; \sum_{n=0}^{+\infty} (1+n^2)^s |\hat{u}_n|^2 < +\infty \right\}.$$

Endowed with the scalar product

$$(u, v)_{T^s} = \hat{u}_0 \overline{\hat{v}_0} + \frac{1}{2} \sum_{n=1}^{+\infty} (1+n^2)^s \hat{u}_n \overline{\hat{v}_n},$$

$T^s$ is a Hilbert space for all $s \geq 0$. Similarly, we set

$$U^s = \left\{ u \in L^2_\omega \;\middle|\; \sum_{n=0}^{+\infty} (1+n^2)^s |\check{u}_n|^2 \right\}$$

which is a Hilbert space for the scalar product

$$(u, v)_{U^s} = \frac{1}{2} \sum_{n=0}^{+\infty} (1+(n+1)^2)^s \check{u}_n \overline{\check{v}_n}.$$

One can extend the definition of $T^s$ ad $U^s$ for $s \in \mathbb{R}$, in which case they form interpolating scales of Hilbert space, see [7] for details. For $s = \pm\frac{1}{2}$, those spaces have been analyzed (with different notation) e.g. in [17] and verify

$$T^{-1/2} = \omega \tilde{H}^{-1/2}(-1,1), \quad T^{1/2} = H^{1/2}(-1,1), \tag{2.3.6}$$

$$U^{-1/2} = H^{-1/2}(-1,1), \quad U^{1/2} = \frac{1}{\omega} \tilde{H}^{1/2}(-1,1). \tag{2.3.7}$$

Denoting by $T^\infty = \cap_{s\geq 0} T^s$ and similarly for $U^\infty$, it is shown in [7] that

**Lemma 2.3.**

$$T^\infty = U^\infty = C^\infty([-1,1]).$$

### 2.3.2 Single layer equation

In the case of Dirichlet condition, we seek a solution to the equation $S_0\lambda = g$, with $\lambda \in \tilde{H}^{-1/2}(\Gamma)$, that is

$$-\frac{1}{2\pi}\int_{-1}^{1} \log|x-y|\lambda(y) = g(x), \quad \forall x \in (-1,1)\,. \tag{2.3.8}$$

This equation is sometimes called "Symm's integral equation" and its resolution has received a lot of attention in the 1990's. Numerical methods, using both the collocation and Galerkin paradigms have been presented and analyzed [6, 35, 41, 42, 43].

Our analysis lies on the following formula. (For a proof, see for example [21] Theorem 9.2. Note that this is also the main ingredient in several connected works, such as [10] and [18].)

**Lemma 2.4.** *For all $n \in \mathbb{N}$, we have*

$$-\frac{1}{2\pi}\int_{-1}^{1} \frac{\ln|x-y|}{\sqrt{1-y^2}} T_n(y)dy = \sigma_n T_n(x)$$

*where*

$$\sigma_n = \begin{cases} \dfrac{\ln(2)}{2} & \text{if } n = 0 \\ \dfrac{1}{2n} & \text{otherwise.} \end{cases}$$

Using the decomposition of $g$ and of the logarithmic kernel on the basis $(T_n)_n$, we see that the solution $\lambda$ to equation (2.3.8) admits the following expansion

$$\lambda(x) = \frac{1}{\sqrt{1-x^2}} \sum_{n=0}^{+\infty} \frac{\hat{g}_n}{\sigma_n} T_n(x)\,. \tag{2.3.9}$$

We deduce the following well-known fact:

**Corollary 2.5.** *If the data $g$ is in $C^\infty([-1,1])$, the solution $\lambda$ to the equation*

$$S_0\lambda = g$$

*is of the form*

$$\lambda(x) = \frac{\alpha(x)}{\sqrt{1-x^2}}$$

*with $\alpha \in C^\infty([-1,1])$.*

*Proof.* Let $\alpha(x) = \sqrt{1-x^2}\,\lambda(x)$ where $\lambda$ is the solution of $S_0\lambda = g$. By Theorem 2.3, if $g \in C^\infty([-1,1])$, then $g \in T^\infty$, and by equation (2.3.9),

$$\hat{\alpha}_n = \frac{\hat{g}_n}{\sigma_n},$$

from which we deduce that $\alpha$ also belongs to $T^\infty = C^\infty([-1,1])$. □

Following [10], we introduce the weighted single layer operator as the operator that appears in Theorem 2.4.

**Definition 2.2.** Let $S_{0,\omega}$ be the weighted single layer operator defined by

$$S_{0,\omega} : \alpha \in C^\infty([-1,1]) \longrightarrow -\frac{1}{2\pi}\int_{-1}^{1} \frac{\ln|x-y|}{\omega(y)}\alpha(y)dy\,.$$

To obtain the solution of (2.3.8), we thus solve

$$S_{0,\omega}\alpha = u_D\,, \tag{2.3.10}$$

and let $\lambda = \frac{\alpha}{\omega}$, which indeed belongs to $\tilde{H}^{-1/2}$ by (2.3.6). From the previous considerations, the inverse for $S_{0,\omega}$ can be derived by building an operator $R$ such that $RT_n = \frac{1}{\sigma_n}T_n$. It turns out that such an operator $R$ has been characterized in [17, 40], through explicit variational forms in closed forms (see also the recent paper [16] for the case of the unit disk in $\mathbb{R}^3$).

Here, we give an alternative form for the operator $R$, that we will then generalize for a non-zero frequency.

**Theorem 2.6.** *For any s, the operator $-(\omega\partial_x)^2 + \frac{1}{\ln(2)^2}\pi_0$ is bicontinuous from $T^{s+2}$ to $T^s$ and*

$$S_{0,\omega}^2 = \frac{1}{4}\left(-(\omega\partial_x)^2 + \frac{1}{\ln(2)^2}\pi_0\right)^{-1}.$$

**Corollary 2.7.** *The operator $S_{0,\omega}$ being non negative, its inverse can thus be equivalently expressed as*

$$S_{0,\omega}^{-1} = R := 2\sqrt{-(\omega\partial_x)^2 + \frac{1}{\ln(2)^2}\pi_0}$$

*where the square root of the operator is defined using standard spectral theory.*

*Proof.* We simply notice that for all $n \in \mathbb{N}$, $(\omega\partial_x)T_n = -n^2T_n$. Therefore

$$\begin{aligned}\left(-(\omega\partial_x)^2 + \frac{1}{\ln(2)^2}\pi_0\right)T_n &= \begin{cases} n^2T_n \text{ if } n \neq 0 \\ \frac{1}{\ln(2)^2} \text{ otherwise} \end{cases} \\ &= \frac{1}{4\sigma_n^2}T_n\,.\end{aligned}$$

□

Since the operator $\sqrt{-(\omega\partial_x)^2 + \frac{1}{\ln(2)^2}\pi_0}$ is the inverse of $S_{0,\omega}$, in particular, it can be used as an efficient preconditioner for the weighted integral equation (2.3.10).

### 2.3.3 Hypersingular equation

We now turn our attention to the equation

$$N_0\mu = g\,. \tag{2.3.11}$$

Similarly to the previous section and following [10], we consider the weighted version of the hypersingular operator $N_{0,\omega} := N_0\omega$ defined by

$$N_{0,\omega}\mu = \lim_{\varepsilon\to 0}\int_{-1}^{1} n(y)\cdot\nabla G(x+\varepsilon n(x)-y)\sqrt{1-y^2}dy\,.$$

We can get the solution to equation (2.3.11) by solving

$$N_{0,\omega}\beta = u_N, \tag{2.3.12}$$

and letting $\mu = \omega\beta$. We now show that $N_{0,\omega}$ can be analyzed using this time the spaces $U^s$.

**Lemma 2.8.** *For any $\beta$, $\beta'$, one has*

$$\left\langle N_{0,\omega}\beta, \beta' \right\rangle_{\omega} = \left\langle S_{0,\omega}\omega\partial_x\omega\beta, \omega\partial_x\omega\beta' \right\rangle_{\frac{1}{\omega}}.$$

*Proof.* We use the well-known integration by part formula

$$\langle N_0 u, v\rangle = \langle S_0\partial_x u, \partial_x v\rangle,$$

valid when $u$ and $v$ are regular enough and vanish at the extremities of the segment. For a smooth $\beta$, we thus have

$$\left\langle N_0(\omega\beta), (\omega\beta')\right\rangle = \left\langle S_0\partial_x(\omega\beta), \partial_x(\omega\beta')\right\rangle$$

which obviously implies the claimed identity. □

**Lemma 2.9.** *For all $n \in \mathbb{N}$, we have*

$$N_{0,\omega}U_n = \frac{n+1}{2}U_n.$$

*Proof.* From the identity $\partial_x T_{n+1} = (n+1)U_n$ and Equation (2.3.1) we obtain

$$\omega\partial_x\omega U_n = -(n+1)T_{n+1}.$$

Therefore, by Theorem 2.8

$$\begin{aligned}\left\langle N_{0,\omega}U_m, U_n\right\rangle_{\omega} &= (n+1)(m+1)\left\langle S_{0,\omega}T_{m+1}, T_{n+1}\right\rangle_{\frac{1}{\omega}} \\ &= \delta_{m=n}\frac{n+1}{2}.\end{aligned} \tag{2.3.13}$$

□

Moreover, recalling that $-(\partial_x\omega)^2U_n = (n+1)^2U_n$ leads to the following Theorem that expresses again the operator $N_\omega$ as a square root operator.

**Theorem 2.10.**

$$N_{0,\omega} = \frac{1}{2}\sqrt{-(\partial_x\omega)^2}. \tag{2.3.14}$$

## 2.4 Helmholtz equation

In this section, we aim at generalizing the preceding analysis to the case of Helmholtz equation on $\mathbb{R}^2 \setminus \Gamma$ with $\Gamma = [-1,1] \times \{0\}$, based on the explicit formulas presented in the previous section. Recall the definition of the single layer and hypersingular operators, $S_k$ and $N_k$, given in (2.2.6) and (2.2.9), and the integral equations (2.2.8) and (2.2.12) for the Dirichlet and Neumann problems respectively. As before, let $S_{k,\omega} := S_k \frac{1}{\omega}$ and $N_{k,\omega} := N_k \omega$. The following commutation holds:

**Theorem 2.11.**

$$S_{k,\omega}\left[-(\omega\partial_x)^2 - k^2\omega^2\right] = \left[-(\omega\partial_x)^2 - k^2\omega^2\right] S_{k,\omega},$$

*Proof.* Since $(\omega\partial_x)^2$ is self adjoint and symmetric (with respect to the bilinear form $(\cdot,\cdot)_{\frac{1}{\omega}}$), we have

$$\left(S_{k,\omega}(\omega\partial_x)^2 u\right)(x) = \int_{-1}^{1} \frac{(\omega_y\partial_y)^2\left[G_k(x-y)\right]u(y)}{\omega(y)},$$

where we use the notation $\omega_y$ and $\partial_y$ to emphasize the dependence in the variable $y$. Thus,

$$\left(\left(S_{k,\omega}(\omega\partial_x)^2 - (\omega\partial_x)^2 S_{k,\omega}\right)u\right)(x) = \int_{-1}^{1} \frac{D_k(x,y)u(y)}{\omega(y)},$$

where $D_k(x,y) := \left[(\omega_y\partial_y)^2 - (\omega_x\partial_x)^2\right]\left[G_k(x-y)\right]$. A simple computation leads to

$$D_k(x,y) = \partial_{xx}G_k(x-y)(\omega_y^2 - \omega_x^2) + \partial_x G_k(x-y)(y+x).$$

Since $G_k$ is a solution of the Helmholtz equation, we have for all $(x \neq y) \in \mathbb{R}^2$

$$\partial_x G_k(x-y) = (y-x)(\partial_{xx}G_k(x-y) + k^2 G(x-y)),$$

thus

$$D_k(x,y) = \partial_{xx}G_k(x-y)\left(\omega_y^2 - \omega_x^2 + y^2 - x^2\right) + k^2(y^2-x^2)G_k(x-y).$$

A careful analysis shows that no Dirac mass appears in the previous formula. Note that $y^2 - x^2 = \omega_x^2 - \omega_y^2$ so the first term vanishes and we find

$$S_{k,\omega}(\omega\partial_x)^2 - (\omega\partial_x)^2 S_{k,\omega} = k^2\left(\omega^2 S_{k,\omega} - S_{k,\omega}\omega^2\right)$$

as claimed. □

There also holds the following identity:

$$N_{k,\omega}\left[-(\partial_x\omega)^2 - k^2\omega^2\right] = \left[-(\partial_x\omega)^2 - k^2\omega^2\right] N_{k,\omega},$$

however, the proof of this commutation is quite heavy. We chose to not include it in the present work for the sake of conciseness.

Those commutations imply that the operators $S_{k,\omega}$ and $N_{k,\omega}$ share the same eigenvectors as, respectively, $\left[-(\omega\partial_x)^2 - k^2\omega^2\right]$ and $\left[-(\partial_x\omega)^2 - k^2\omega^2\right]$. The eigenfunctions of the operator $\left[-(\omega\partial_x)^2 - k^2\omega^2\right]$ thus provide us with a diagonal basis for $S_{k,\omega}$. They are the solutions to the differential equation

$$(1-x^2)\partial_{xx}y - x\partial_x y - k^2\omega^2 y = \lambda y.$$

Once we set $x = \cos\theta$, $\tilde{y}(\theta) = y(x)$, $q = \frac{k^2}{4}$, $a = \lambda + 2q$, $\tilde{y}$ is a solution of the standard Mathieu equation

$$\tilde{y}'' + (a - 2q\cos(2\theta))\tilde{y} = 0\,. \tag{2.4.1}$$

There exists a discrete set of values $a_{2n}(q)$ for which this equation possesses even and $2\pi$ periodic solutions, which are known as the Mathieu cosine functions, and usually denoted by $\mathrm{ce}_n$. Here, we use the notation $\mathrm{ce}_n^k$ to emphasize the dependency in the parameter $k = \sqrt{2q}$ of those functions. The normalization is taken as

$$\int_{-\pi}^{\pi} \mathrm{ce}_n^k(\theta)^2 d\theta = \pi.$$

The Mathieu cosine functions also satisfy

$$\int_{-\pi}^{\pi} \mathrm{ce}_n^k(\theta)\mathrm{ce}_m^k(\theta) = \pi\delta_{m,n}$$

so that any even $2\pi$ periodic function in $L^2(-\pi,\pi)$ can be expanded along the functions $\mathrm{ce}_n$, with the coefficients obtained by orthonormal projection. Setting

$$T_n^k := \mathrm{ce}_n^k(\arccos(x)),$$

in analogy to the zero-frequency case, we have

$$\left[-(\omega\partial_x)^2 - k^2\omega^2\right] T_n^k = \lambda_{n,k}^2 T_n^k.$$

For large $n$, using the general results from the theory of Hill's equations (see e.g. [27, eq. (21), (28) and (29)]), we have the following asymptotic formula for $\lambda_{n,k}$:

$$\lambda_{n,k}^2 = n^2 - \frac{k^4}{16n^2} + o\left(n^{-2}\right).$$

The first commutation established in Theorem 2.11 implies that Mathieu cosine functions are also the eigenfunctions of the single-layer operator. (An equivalent statement is given in [9, Thm 4.2], if we allow the degenerate case $\mu = 0$.)

A similar analysis can be applied to the hypersingular operator. The eigenfunctions of $\left[-(\partial_x\omega)^2 - k^2\omega^2\right]$ are given by

$$U_n^k := \frac{\mathrm{se}_n^k(\arccos(x))}{\omega(x)}$$

where $\mathrm{se}_n^k$ are the so-called Mathieu sine functions, which also satisfy the Mathieu differential equation (2.4.1), but with the condition that they are $2\pi$ periodic and odd functions.

All the previous considerations highly suggest the following theorem:

**Theorem 2.12.** *There exists a compact operator $K$ from $T^s$ to $T^{s+2}$ such that*

$$\left[-(\omega\partial_x)^2 - k^2\omega^2\right] S_{k,\omega}^2 = \frac{I_d}{4} + K,$$

*and a compact operator $K'$ from $U^s$ to $U^{s-2}$ such that*

$$N_{k,\omega}^2 = \left[-(\partial_x\omega)^2 - k^2\omega^2\right] + K'.$$

The proof of this theorem, requires the introduction of additional analytic tools that are out of the scope of this introductory paper. It is thus omitted in the present work and given in full details in [7]. Nevertheless, Theorem 2.12 gives a generalization to Helmholtz equation of the result obtained precedingly for Laplace equation, namely, the operator $\left[-(\omega\partial_x)^2 - k^2\omega^2\right]^{1/2}$ is expected to be a good preconditioner for $S_{k,\omega}$, as well as $\left[-(\partial_x\omega)^2 - k^2\omega^2\right]^{-1/2}$ for $N_{k,\omega}$.

Finally, we note that in the more general case of a $C^\infty$ non-intersecting open curve $\Gamma$ and non-zero frequency $k$, the previous result extends, replacing $\partial_x$ by $\partial_\tau$ the tangential derivative on $\Gamma$, $S_{k,\omega}$ and $N_{k,\omega}$ respectively by $S_{k,\omega_\Gamma} := S_k \frac{1}{\omega_\Gamma}$, and $N_{k,\omega_\Gamma} := N_k \omega_\Gamma$, and $\omega$ by $\omega_\Gamma$. Here $\omega_\Gamma$ is defined by $\omega_\Gamma(x) = \frac{|\Gamma|}{2}\omega(r(x))$, where $|\Gamma|$ is the length of the curve and $r : [-1,1] \to \Gamma$ is such that for all $x$, $|\partial_x r(x)| = \frac{|\Gamma|}{2}$.

## 2.5 Numerical results

### 2.5.1 Galerkin setting

To solve numerically the integral equations presented earlier, various methods have been described and analyzed in the literature. The standard discretization on a uniform mesh with piecewise polynomial trial functions leads to very poor rates of convergence (see for example [32, Chap. 4]). Several strategies have been developed to remedy this problem. One can for example enrich the trial space with special singular functions, refine the mesh near the segment tips (h-BEM) or increase the polynomial order in the trial space (p-BEM). The combination of the last two methods, known as h-p BEM, can achieve an exponential rate of convergence with respect to the dimension of the trial space, see [29] and references therein. Spectral methods, involving trigonometric polynomials have also been analyzed for example in [10], and some results exist for piecewise linear functions in the colocation setting [12].

Here, we describe a simple Galerkin setting, suited to the spaces $T^s$ and $U^s$. We use simple piecewise affine functions defined on a non-uniform mesh, which is refined towards the edges of the curve. More precisely, let $-1 = x_0 < x_1 < \cdots < x_N = 1$ and let $\theta_i := \arccos(x_i)$. We choose the points $x_i$ such that $(\theta_i)_{0\le i\le N}$ are equispaced, that is to say $\theta_i = ih$ with $h = \pi/N$. The nodes of the mesh are then set to $X_i = r(x_i)$, where $r$ is a smooth parametrization of the curve $\Gamma$. This turns out to be analogous to a graded mesh with a grading parameter equal to 2 which means that, near the edge, the width of the $i-th$ interval is approximately $(ih)^2$. Notice that it is known that this modification alone, i.e. using the h-BEM method with a polynomial order $p = 1$, is not sufficient to get an optimal rate of convergence. Indeed, it can be shown that it only leads to a convergence rate in $O(h)$ for the $L^2$ norm (cf. [29, Theorem 1.3]) instead of the expected $O(h^2)$ behavior.

The key ingredient, beside the graded mesh, to recover optimal convergence is to use a weighted $L^2$ scalar product (with weight $\frac{1}{\omega}$ or $\omega$ depending on the considered equation), in order to assemble the operators in their natural spaces. We state here the orders of convergence that one gets with this new method, and refer again the reader to [7] for rigorous proofs. To keep the exposition simple, we also restrict our presentation to the case where $\Gamma = [-1,1]\times\{0\}$ and $k = 0$.

**Dirichlet problem** For the of resolution the single-layer equation (2.3.8) we use a variational formulation of (2.3.10) to compute an approximation $\alpha_h$ of $\alpha$. Namely, let $V_h$ the Galerkin space of (discontinuous) piecewise affine functions defined on the mesh $(x_i)_{0\le i\le N}$ defined above, and $\alpha_h$ the

unique solution in $V_h$ to

$$\left(S_{0,\omega}\alpha_h, \alpha_h'\right)_{\frac{1}{\omega}} = \left(u_D, \alpha_h'\right)_{\frac{1}{\omega}}, \quad \forall \alpha_h' \in V_h.$$

We then compute $\lambda_h = \frac{\alpha_h}{\omega}$. Using the notation $C$ to denote any constant that does not depend on the relevant parameters, we then have

**Theorem 2.13.** *(see [7]). If the data $u_D$ is in $T^{s+1}$ for some $-1/2 \leq s \leq 2$, then there holds:*

$$\|\lambda - \lambda_h\|_{\tilde{H}^{-1/2}} \leq Ch^{s+1/2} \|\omega\lambda\|_{T^s} \leq Ch^{s+1/2} \|u_D\|_{T^{s+1}}.$$

In particular, when $u_D$ is smooth, the solution $\alpha = \omega\lambda$ belongs to $T^\infty$, and we get the optimal rate of convergence of the error in $O(h^{5/2})$.

**Neumann problem.** For the numerical resolution of (2.3.11), we use a variational form for equation (2.3.12) to compute an approximation $\beta_h$ of $\beta$, and solve it using a Galerkin method with continuous piecewise affine functions. Introducing $W_h$ the space of continuous piecewise affine functions on the mesh defined by the points $(x_i)_{0\leq i\leq N}$, we denote by $\beta_h$ the unique solution in $W_h$ to the variational equation:

$$\left(N_\omega\beta_h, \beta_h'\right)_\omega = \left(u_N, \beta_h'\right)_\omega, \quad \forall \beta_h' \in W_h. \tag{2.5.1}$$

Then, the proposed approximation for $\mu$, given by $\mu_h = \omega\beta_h$, satisfies the following error estimate.

**Theorem 2.14.** *(see [7]). If $u_N \in U^{s-1}$, for some $\frac{1}{2} \leq s \leq 2$, there holds*

$$\|\mu - \mu_h\|_{\tilde{H}^{1/2}} \leq Ch^{s-\frac{1}{2}} \left\|\frac{\mu}{\omega}\right\|_{U^s} \leq Ch^{s-\frac{1}{2}} \|u_N\|_{U^{s-1}}.$$

In fact, in [7], we prove that, for the Dirichlet problem,

$$\forall s,t \in \left[-\frac{1}{2}, 2\right], \quad \|\alpha - \alpha_h\|_{T^t} \leq Ch^{s-t} \|\alpha\|_{T^s}.$$

The case $t = 0$ gives a convergence rate in $O(h^s)$ for the weighted $L^2$ error $e_1(h) = \|\alpha - \alpha_h\|_{L^2_{\frac{1}{\omega}}}$, where $s$ is such that $\alpha \in T^s$. A numerical validation is shown in Figure 2.1. We consider here the case where $\alpha_1(x) = \omega(x) \in T^s$ for $s < \frac{3}{2}$ and $\alpha_1 \notin T^{3/2}$ and $\alpha_2 = \omega(x)^3 \in T^2$. We indeed observe the respective rates $O(h^{3/2})$ and $O(h^2)$ predicted by the theory.
Similarly for the Neumann case it is shown in [7] that

$$\forall s,t \in [0,2], \quad \|\beta - \beta_h\|_{U^t} \leq Ch^{s-t} \|\beta\|_{U^s} \tag{2.5.2}$$

A numerical validation is shown in Figure 2.2 in the case $\beta = U_2 \in U^\infty$.The error in $L^2_\omega$ and $U^1$ norms are plotted, and the rates of convergence observed predicted by the theory are recovered in practice.

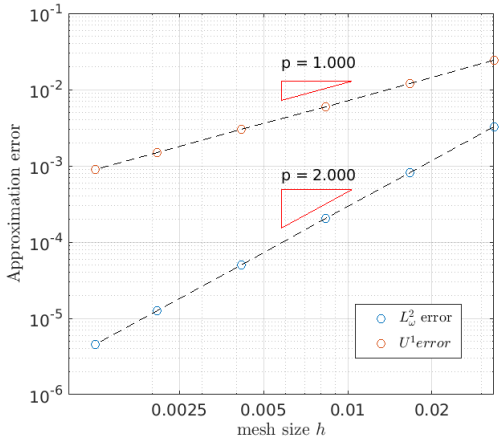


Figure 2.2: Effective order of convergence of the approximation of the solution $\beta$ to (2.3.12) by the weighted Galerkin method. The second member is taken as $u_N = U_2 \in U^\infty$, and the solution is therefore $\beta = \frac{2}{3}U_2$. We plot in blue the $L^2_\omega$ error $\|\beta - \beta_h\|_\omega$ and in red the $U^1$ error $\|\beta - \beta_h\|_{U^1}$. Here the theory predicts the $O(h)$ order of convergence for the second curve. The $O(h^2)$ order of the first curve is not yet explained by our theory.

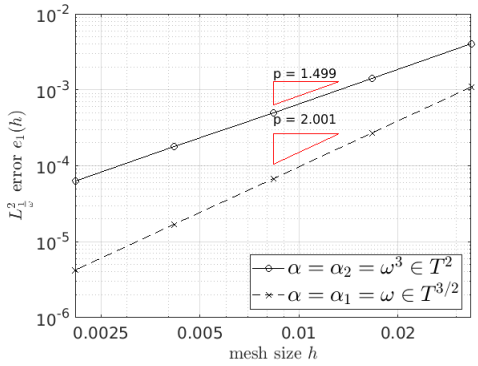


Figure 2.1: Effective order of convergence of the approximation of the solution $\alpha$ to (2.3.10) by the weighted Galerkin method. The blue data correspond to a case where $\alpha \in T^s$ for all $s < \frac{3}{2}$ but $\alpha \notin T^{3/2}$. In this case, the theory predicts a $O(h^{3/2})$ rate of convergence, which is what we observe in practice. The red data corresponds to a case where $\alpha \in T^s$. In this case, a $O(h^2)$ rate of convergence is predicted by the theory and indeed observed here.

### 2.5.2 Preconditioning the linear systems

Let $X_h$ the considered finite element space ($X_h = V_h$ or $W_h$), and $(\phi_i)_i$ the basis functions. For an operator $A$, we denote by $[A]_p$ the Galerkin matrix of the operator for the relevant weight $p(x) = \frac{1}{\omega(x)}$ or $\omega(x)$, defined by

$$[A]_{p,ij} = \int_\Gamma (A\phi_j)(x)\phi_i(x)p(x)\,dx\,.$$

When the operator $BA$ is a compact perturbation of the identity (either in $T^s$ or $U^s$) then, following [36], we precondition the linear system $[A]_p x = b$ by the matrix $[I_d]_p^{-1}[B]_p[I_d]_p^{-1}$, which amounts to

solve

$$[I_d]_p^{-1}[B]_p[I_d]_p^{-1}[A]_p x = [I_d]_p^{-1}[B]_p[I_d]_p^{-1} b\,.$$

When $B$ is the inverse of a local operator $C$, then it may be more convenient to compute $[C]_p$, and solve instead

$$[C]_p^{-1}[A]_p x = [C]_p^{-1} b\,.$$

The preconditioners introduced in this work are in the form of square roots of local operators. More precisely, we introduced two preconditioners $P_1$ and $P_2$ with

$$\begin{aligned} P_1(k) &= \left(-(\omega\partial_x)^2 - k^2\omega^2\right)^{1/2} \\ P_2(k) &= \left(-(\partial_x\omega)^2 - k^2\omega^2\right)^{-1/2} \end{aligned}$$

For the second equation, we rewrite

$$P_2(k) = \left(-(\partial_x\omega)^2 - k^2\omega^2\right)^{-1}\left(-(\partial_x\omega)^2 - k^2\omega^2\right)^{1/2},$$

which brings us back to computing the square root of a sparse matrix. When the frequency is 0, we use the method exposed in [14]. When the frequency is non-zero, the previous method fails since the spectrum of the matrix contains negative values. In [5], a method involving a Padé approximation of the square root, with a rotated branch cut, is used to compute the matrix of an operator of the form $\sqrt{X - k^2 I_d}$ where $X$ is a positive definite operator. This method gives excellent results in our context when using $X = -(\partial\omega_x)^2 + k^2\left(I_d - \omega^2\right)$. Specifically, we build a rational approximation of the function $X \mapsto \sqrt{X - k^2}$ in the form

$$\sqrt{X - k^2} = a_0 + \sum_{i=0}^{N_p} \frac{a_i}{b_i + X}\,.$$

We then take

$$\left[\sqrt{X - k^2 I_d}\right]_p \approx a_0[I_d]_p + \sum_{i=0}^{N_p} a_i\left(b_i[I_d]_p + [X]_p\right)^{-1}\,.$$

### 2.5.3 Numerical results

All the numerical results exposed here are obtained on a personal laptop running on an eight cores intel i7 processor with a clock rate of 2.8GHz. The Galerkin method has been implemented in the language Matlab R2018.

**Flat segment, Laplace-Dirichlet problem.** In Table 2.1, we report the number of iterations for the numerical resolution of the Laplace problem (2.3.10) by the method detailed above, in Section 2.5. Two cases are considered, first without any preconditioner, and then with a preconditioner given by $[I_d]_{\frac{1}{\omega}}^{-1}[B]_{\frac{1}{\omega}}[I_d]_{\frac{1}{\omega}}^{-1}$ where $[B]_{\frac{1}{\omega}}$ is the Galerkin matrix of the operator $\sqrt{-(\omega\partial_x)^2 + \frac{1}{\ln(2)^2}\pi_0}$. The right hand side in (2.3.10) is chosen as $u_D(x) = (x^2 + 0.001)^{-1/2}, x \in [-1,1]$. A graph of the residual along the iterations is given in Figure 2.3 for a graded mesh with 1600 node points.

| | with Prec. | | without Prec. | |
|---|---|---|---|---|
| $N$ | $n_{it}$ | t(s) | $n_{it}$ | t(s) |
| 50 | 7 | 0.11 | 35 | 0.21 |
| 200 | 7 | 0.14 | 53 | 0.55 |
| 800 | 7 | 0.29 | 76 | 2.0 |
| 3200 | 7 | 0.95 | 107 | 9.5 |

Table 2.1: Number of iteration and time needed for the numerical resolution of (2.3.10) using Galerkin finite elements with and without preconditioner.

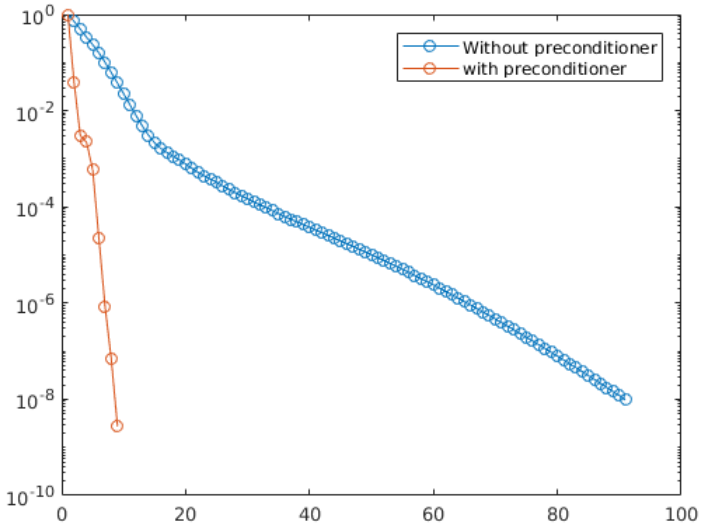


Figure 2.3: Number of iteration in the resolution of the single layer integral equation with a mesh of size $N = 1600$.

**Flat segment, Laplace-Neumann problem.** For the Neumann problem (2.3.12), we also report in Table 2.2 the number of iterations for the numerical resolution with and without the preconditioner given by $[I_p]_\omega^{-1}[C]_\omega[I_p]_\omega^{-1}$ where $[C]_\omega$ is the Galerkin matrix of the operator $\sqrt{-(\partial_x\omega)^{-2}}$. The right hand side in (2.3.12) is chosen as $u_N(x) = (x^2+0.001)^{1/2}, x \in [-1,1]$. The decay of the residual along the iterations is shown in Fig. 2.4.

| | with Prec. | | without Prec. | |
|---|---|---|---|---|
| $N$ | $n_{it}$ | t(s) | $n_{it}$ | t(s) |
| 50 | 4 | 0.09 | 50 | 0.31 |
| 200 | 4 | 0.12 | 200 | 2.0 |
| 800 | 4 | 0.56 | 799 | 30 |
| 3200 | 4 | 17.7 | 3007 | 630 |

Table 2.2: Number of iteration and time needed for the numerical resolution of (2.3.10) using Galerkin finite elements with and without preconditioner.

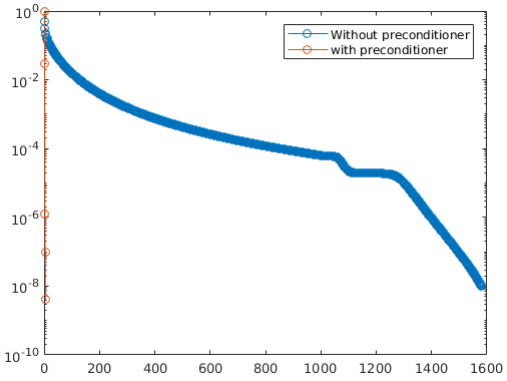


Figure 2.4: Number of iteration in the resolution of the hypersingular integral equation with a mesh of size $N = 1600$. The importance of preconditioning in this case is even more spectacular than in the case of the single-layer equation.

We observe in both Dirichlet and Neumann cases a drastic decay of the number of iteration which justifies the approach. We also see that, as expected, the number of iterations obtained with the preconditioned version does not depend on the mesh.

We now turn our attention to Helmholtz equation. In each case, in order to fully resolve the frequency, the number of segments in the discretization is set to $N \approx 10k$, where $k = \frac{\pi}{\lambda}$ is the wavenumber. In the GMRES iteration, we require a relative residual below $10^{-8}$.

**Flat segment, Helmholtz-Dirichlet problem.** In Table 2.3 we report the number of GMRES iterations for the numerical resolution of Equation (2.2.8) on the segment $\Gamma = [-1,1] \times \{0\}$, when the linear system is preconditioned by the operator $\sqrt{-(\omega\partial_x)^2 - k^2\omega^2}$, as compared to the case where no preconditioner is used. We take, for the Dirichlet data, the plane wave $u_D(x) = e^{ikx}$. We also provide, in Figure 2.5, the value of the relative residual in the GMRES method along the iterations, with and without preconditioner, for a problem with $L = 800\lambda$. As before, we see that the number of iterations needed to reach a given precision decreases significantly but, this time, we observe a very slight increase with respect to the wavenumber.

| | with Prec. | | without Prec. | |
|---|---|---|---|---|
| $L/\lambda$ | $n_{it}$ | t(s) | $n_{it}$ | t(s) |
| 50 | 8 | 0.1 | 73 | 0.28 |
| 200 | 10 | 1.3 | 116 | 17 |
| 800 | 15 | 34 | 148 | 300 |

Table 2.3: Number of iterations and time needed for the numerical resolution of (2.3.10) using Galerkin finite elements with and without preconditioner.

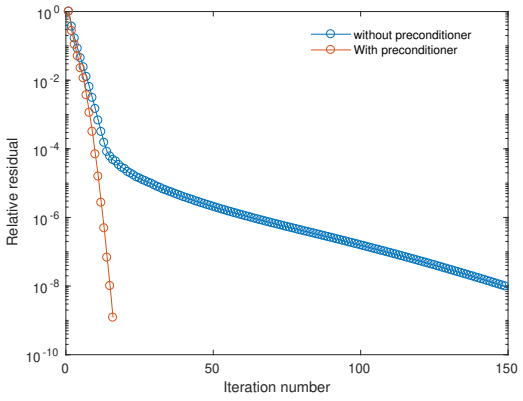


Figure 2.5: Number of iteration in the resolution of the single layer integral equation with a mesh of size $N \approx 3700$, $L = 800\lambda$.

**Flat segment, Helmholtz-Neumann problem.** Finally, to end up this validation stage, we run the same numerical comparisons, this time solving (2.2.12) and considering the preconditioning operator $\left(-(\partial_x \omega)^2 - k^2\omega^2\right)^{-1/2}$. Results are given in Table 2.4 for different meshes and in Figure 2.6 for the evolution of the residual along the iterations. Huge differences, btoh in time and number of iterations are shown in favor of the preconditioned system.

| | with Prec. | | without Prec. | |
|---|---|---|---|---|
| $L/\lambda$ | $n_{it}$ | t(s) | $n_{it}$ | t(s) |
| 50 | 8 | 0.08 | 785 | 9.4 |
| 200 | 10 | 3.6 | $> 2000$ | $>$ 2min |
| 800 | 17 | 73 | $> 2000$ | $>$ 2min |

Table 2.4: Number of iteration and time needed for the numerical resolution of (2.3.10) using Galerkin finite elements with and without preconditioner.

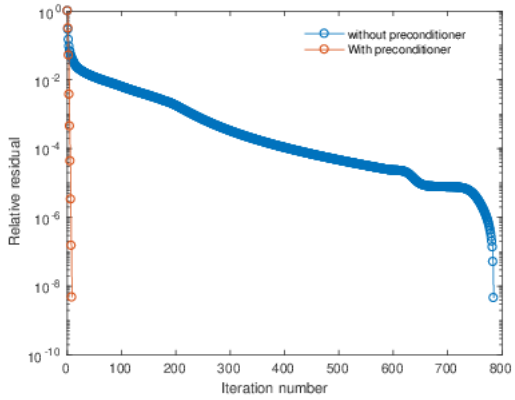


Figure 2.6: Number of iteration in the resolution of Hypersingular integral equation with a mesh of size $N \approx 800$, $L = 50\lambda$.

**Non-flat arc.** Here, we also report numerical results when the curve is a portion of spiral (see Figure 2.7), for both boundary conditions. This shows that the preconditioning strategy is also efficient in presence of non-zero curvature.

| | With prec. | | Without prec. | |
|---|---|---|---|---|
| $L/\lambda$ | $n_{it}$ | t(s) | $n_{it}$ | t(s) |
| 50 | 23 | 0.6 | 785 | 9.4 |
| 200 | 27 | 9 | $> 2000$ | $>$ 2min |
| 800 | 40 | 35 | $> 2000$ | $>$ 2min |

Table 2.5: Computing times and number of iterations for the spiral-shaped arc.

**Comparison with the generalized Calderon relations.** Eventually, we test the idea that was presented in [10], namely to use $S_{k,\omega}$ and $N_{k,\omega}$ as mutual preconditioners. This alternative method is also very efficient in our numerical setting (here, we use simple piecewise affine functions, whereas in [10], spectral discretization with trigonometric polynomials is used). We report in Table 2.6 the number of iterations and computing times for the Neumann problem with an angle of incidence $\frac{\pi}{4}$ on the flat segment. The number of iterations is comparable for both methods. However, the matrix-vector product time in our method is significantly slower as it only involves sparse operators. This leads to a faster resolution of the linear system.

| | Calderon Prec. | | Square root Prec. | |
|---|---|---|---|---|
| $L/\lambda$ | $n_{it}$ | t(s) | $n_{it}$ | t(s) |
| 50 | 14 | 0.1 | 8 | 0.1 |
| 200 | 15 | 7.5 | 11 | 3.6 |
| 800 | 16 | 130 | 15 | 70 |

Table 2.6: Number of iteration and time needed for the numerical resolution of (2.2.8) using Galerkin finite elements with and without preconditioner.

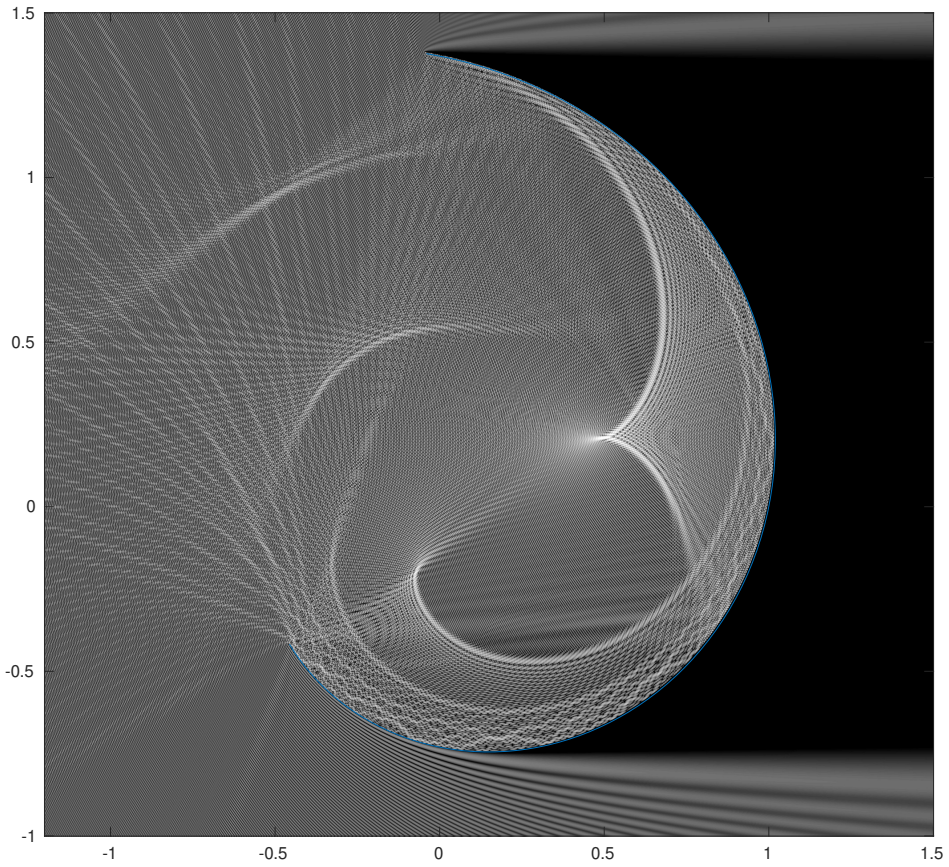


Figure 2.7: Sample diffraction pattern (Dirichlet boundary conditions) with left to right incidence for an arc of spiral of size $L = 800\lambda$. After the resolution of the integral equation, the computation of the image is accelerated by the EBD method [8].

## 2.6 Conclusion

We have presented a new approach for the preconditioning of integral equations coming from the discretization of wave scattering problems in 2D by open arc domains. The methodology is very effective and proven to be optimal for Laplace problems on straight segments. It has three advantages:

- It generalizes the formulas mainly proposed in [5] for regular domains, which is only modified by a suitable weight.
- We can show that one can recover optimal error estimates, provided that the mesh is suitably graded near the edges.
- Eventually, a novel pseudo-differential approach, adapted to the corner singularities that appear in the problem is proposed. It is sketched in the present paper, but given in full details in [7].

We deeply believe that the methodology opens new perspectives for such problems. First, a generalization to specific 3D scattering problem, e.g. by a flat disc seems a simple generalization. We plan

to extend the results presented here to such problems in the very near future. Second, the strategy that we used here seems very likely to be extended to the half line and hopefully to 2D sectors, giving, on the one hand a new pseudo-differential analysis more suitable than classical ones (see e.g. [24, 28, 33, 34]) for handling Helmholtz-like problems on singular domains, and, on the other hand, a completely new preconditioning technique adapted to the treatment of BEM operators on domains with corners or wedges in 3D. Eventually, the weighted square root operators that appeared in the present context might well be generalized to give suitable approximation of the exterior Dirichlet to Neumann map for the Helmholtz equation which is of particular importance in e.g. domain decomposition methods. Having such approximations might therefore lead to better methods in that context too.

# Bibliography

[1] F. Alouges and M. Aussal. The Sparse Cardinal Sine Decomposition and its application for fast numerical convolution. *Numerical Algorithms*, 70(2), 2015.

[2] F. Alouges, J. Bourguignon-Mirebeau and D. Levadoux. A simple preconditioned domain decomposition method for electromagnetic scattering problems. *J. Comput. Math.*, 31(1), 2013.

[3] F. Alouges, S. Borel and D. Levadoux. A Stable well conditioned integral equation for electromagnetism scattering, *J. Comput. Appl. Math.* 204(2):440–451, 2007.

[4] F. Alouges, S. Borel and D. Levadoux. A new well-conditioned integral formulation for Maxwell equations in three-dimensions. *IEEE Trans. on Antennas and Propagation* 53(9), 2005.

[5] X. Antoine and M. Darbas. Generalized combined field integral equations for the iterative solution of the three-dimensional helmholtz equation. *ESAIM: Mathematical Modelling and Numerical Analysis*, 41(1):147–167, 2007.

[6] K. E. Atkinson and I. H. Sloan. The numerical solution of first-kind logarithmic-kernel integral equations on smooth open arcs. *mathematics of computation*, 56(193):119–139, 1991.

[7] M. Averseng, New preconditioners for Laplace and Helmholtz integral equation on open curves: II. Theoretical analysis. *Submitted*.

[8] M. Averseng. Fast discrete convolution in $\mathbb{R}^2$ using sparse Bessel Decomposition. accepted for publication in *Numerical Algorithms*, 2018 and *arXiv:1711.07877 [math.NA]*, 2017.

[9] T. Betcke, J. Phillips, and E. A. Spence. Spectral decompositions and nonnormality of boundary integral operators in acoustic scattering. *IMA Journal of Numerical Analysis*, 34(2):700–731, 2014.

[10] O. P. Bruno and S. K. Lintner. Second-kind integral solvers for te and tm problems of diffraction by open arcs. *Radio Science*, 47(6), 2012.

[11] S. H. Christiansen and J.-C. Nédélec. A preconditioner for the electric field integral equation based on calderon formulas. *SIAM Journal on Numerical Analysis*, 40(3):1100–1135, 2002.

[12] M. Costabel, V. J. Ervin, and E. P. Stephan. On the convergence of collocation methods for Symm's integral equation on open curves. *Mathematics of computation*, 51(183):167–179, 1988.

[13] M. Darbas. Generalized combined field integral equations for the iterative solution of the three-dimensional maxwell equations. *Applied Mathematics Letters*, 19(8):834–839, 2006.

[14] N. Hale, N. J. Higham, and L. N. Trefethen. Computing aˆ$\alpha$,\log(a), and related matrix functions by contour integrals. *SIAM Journal on Numerical Analysis*, 46(5):2505–2523, 2008.

[15] R. Hiptmair, C. Jerez-Hanckes, and C. Urzua-Torres. Mesh-independent operator preconditioning for boundary elements on open curves. *SIAM Journal on Numerical Analysis*, 52(5):2295–2314, 2014.

[16] R. Hiptmair, C. Jerez-Hanckes, and C. Urzua-Torres. Closed-form exact inverses of the weakly singular and hypersingular operators on disks. *arXiv preprint arXiv:1703.08556*, 2017.

[17] C. Jerez-Hanckes and J.-C. Nédélec. Explicit variational forms for the inverses of integral logarithmic operators over an interval. *SIAM Journal on Mathematical Analysis*, 44(4):2666–2694, 2012.

[18] S. Jiang and V. Rokhlin. Second kind integral equations for the classical potential theory on open surfaces ii. *Journal of Computational Physics*, 195(1):1–16, 2004.

[19] D. P. Levadoux. Some preconditioners for the CFIE equation of electromagnetism. *Math. Meth. Appl. Sci.*, 17:2015–2028, 2008.

[20] D. P. Levadoux, F. Millot, and S. Pernet. New trends in the preconditioning of integral equations of electromagnetism. *Springer-Verlag Berlin Heifelberg*, Scientific Computing in Electrical Engineering SCEE 2008 by Janne Roos, Luis R. J. Costa (Mathematics in industry 14) 383–394, 2010.

[21] J. C. Mason and D. C. Handscomb. *Chebyshev polynomials*. CRC Press, 2002.

[22] W. C. H. McLean. *Strongly elliptic systems and boundary integral equations*. Cambridge university press, 2000.

[23] W. C. H. McLean, T. Tran. A preconditioning strategy for boundary element galerkin methods. *Numer. Methods for Partial Differential Equations*, 13:283–301 1997.

[24] R. Melrose. Transformation of boundary problems. *Acta Mathematica*. 147:149–236, 1981.

[25] Lars Mönch. On the numerical solution of the direct scattering problem for an open sound-hard arc. *Journal of computational and applied mathematics*, 71(2):343–356, 1996.

[26] J.-C. Nedelec. *Acoustic and Electromagnetic Equations, integral representations for harmonic problems*. Springer, 2001.

[27] F. W. J. Olver, A. B. Olde Daalhuis, D. W. Lozier, B. I. Schneider, R. F. Boisvert, C. W. Clark, B. R. Miller, and B. V. Saunders. *NIST Digital Library of Mathematical Functions*. http://dlmf.nist.gov/, Release 1.0.16 of 2017-09-18.

[28] P. Ola and L. Päivärinta, *Mellin operators and pseudodifferential operators on graphs*, Waves Random Media **14** (2004) S129-S142.

[29] F. V. Postell and E. P. Stephan. On the h-, p-and hp versions of the boundary element method?numerical results. *Computer Methods in Applied Mechanics and Engineering*, 83(1):69–89, 1990.

[30] P. Ramaciotti and J.-C. Nédélec. About some boundary integral operators on the unit disk related to the laplace equation. *SIAM Journal on Numerical Analysis*, 55(4):1892–1914, 2017.

[31] Y. Saad and M. H. Schultz. GMRES: A generalized minimal residual algorithm for solving nonsymmetric linear systems. *SIAM J. Sci. Stat. Comput.*, 7:856–869, 1986.

[32] S. A. Sauter and C. Schwab. Boundary element methods. *Boundary Element Methods*, pages 183–287, 2011.

[33] S. Rempel and B. Schulze. Parametrices and boundary symbolic calculus for elliptic boundary problems without the transmission property, *Math. Nachr.* 105:45–149, 1982.

[34] S. Rempel and B. Schulze. Asymptotics for elliptic mixed boundary problems. Pseudo-differential and Mellin operators in spaces with conormal singularity. *Mathematical Research* 50, 1989.

[35] I. H. Sloan and E. P. Stephan. Collocation with chebyshev polynomials for symm's integral equation on an interval. *The ANZIAM Journal*, 34(2):199–211, 1992.

[36] O. Steinbach and W. L. Wendland. The construction of some efficient preconditioners in the boundary element method. *Advances in Computational Mathematics*, 9(1-2):191–216, 1998.

[37] E. P. Stephan and W. L. Wendland. An augmented galerkin procedure for the boundary integral method applied to two-dimensional screen and crack problems. *Applicable Analysis*, 18(3):183–219, 1984.

[38] O. Steinbach and W.L. Wendland. The construction of some efficient preconditioners in the boundary element method. *Adv. Comput. Math.*, 9(1–2):191–216, 1998.

[39] E. P. Stephan and W. L. Wendland. A hypersingular boundary integral method for two-dimensional screen and crack problems. *Archive for Rational Mechanics and Analysis*, 112(4):363–390, 1990.

[40] C. A. Urzúa Torres et al. Optimal preconditioners for solving two-dimensional fractures and screens using boundary elements. 2014.

[41] Y. Yan and I. H. Sloan. Mesh grading for integral equations of the first kind with logarithmic kernel. *SIAM journal on numerical analysis*, 26(3):574–587, 1989.

[42] Y. Yan, I. H Sloan, et al. *On integral equations of the first kind with logarithmic kernels*. University of NSW, 1988.

[43] Y. Yan. Cosine change of variable for symm's integral equation on open arcs. *IMA Journal of Numerical Analysis*, 10(4):521–535, 1990.